Department of Precision and Microsystems Engineering

Enhancing the Q Factor of Diamagnetically Levitating Resonators by Segmentation

Eli Weisz

Report no : 2023.078
Coach : Xianfeng Chen
Professor : Farbod Alijani
Specialisation : Mechatronic System Design
Type of report : MSc Thesis
Date : August 24, 2023

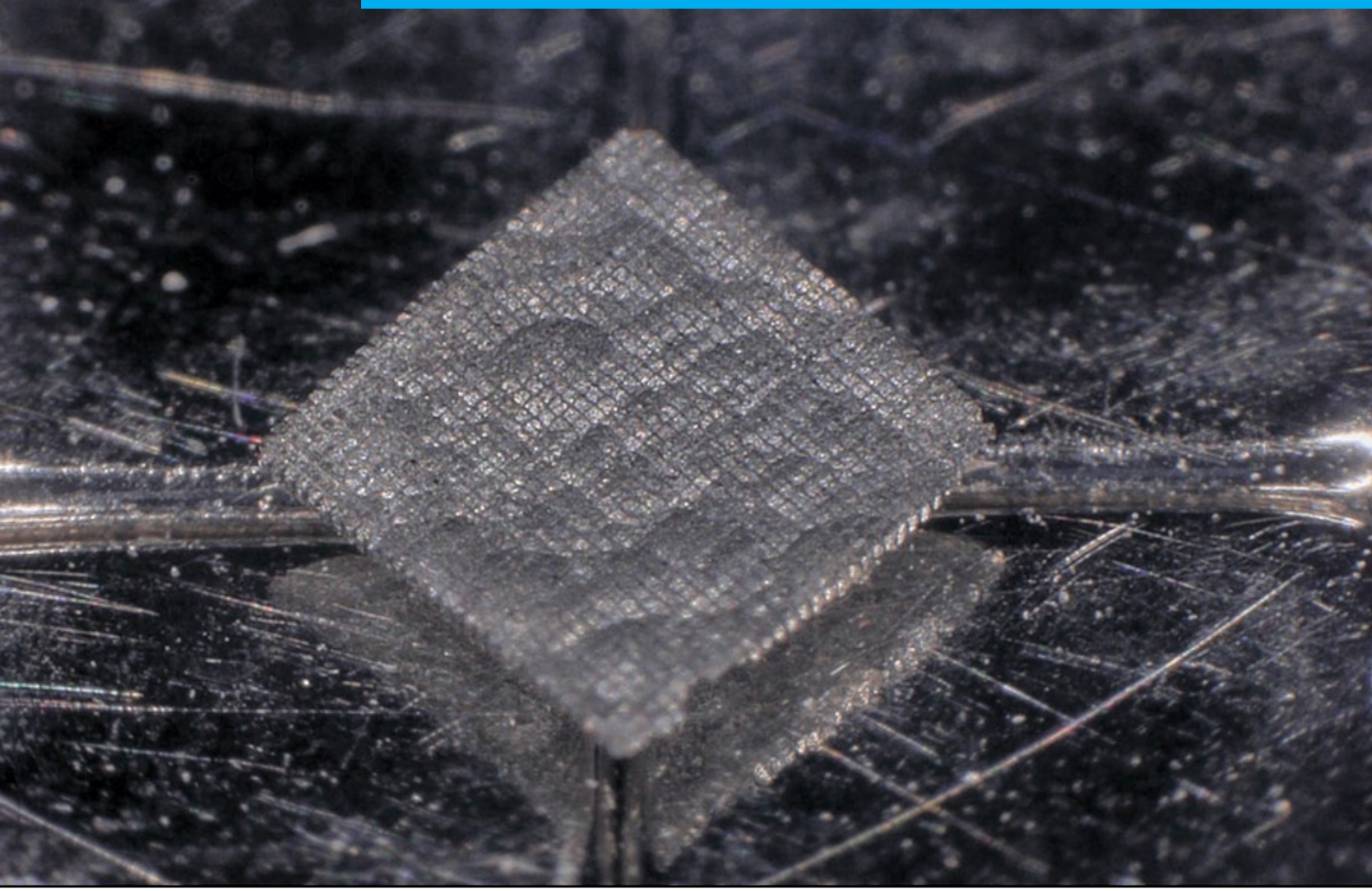

TU Delft Delft University of Technology

Challenge the future

Contents

List of Figures

List of Tables

Chapter 1

Introduction

Levitation of micro- and nano-objects has been a topic of great interest among scientists, with various physical phenomena employed for stable levitation. Some of the commonly used techniques include magnetic levitation, electric levitation, optical levitation, and acoustic levitation[1]. These techniques have found applications in diverse fields such as containerless processing, material investigation, frictionless bearings, high-speed transportation, spectroscopy, sensors, and energy harvesting[1,2].

In the realm of magnetic levitation, different approaches are encompassed, including the use of permanent magnets, electromagnets, superconductors, and diamagnetic materials. While stable levitation with regular magnets alone is not possible due to Earnshaw's theorem, stabilization techniques such as rotation or mechanical support can be employed to achieve pseudo-levitation[3]. On the other hand, superconductive levitation, also known as quantum levitation or quantum locking, takes advantage of the Meissner effect exhibited by superconductors, allowing them to levitate above or below a magnet. This form of levitation provides stability and vibrational freedom, making it suitable for various applications[4]. Furthermore, diamagnetic levitation exploits the repulsive force experienced by materials with a greater diamagnetic effect than magnetic effect, enabling stable and free levitation without the need for additional stabilization techniques[5].

Another method of levitation is electric levitation, which involves the levitation of charged particles in an electric field. Electrostatic levitation, a form of electric levitation, requires stabilization techniques due to Earnshaw's theorem. The quadrupole ion trap, also known as a Paul trap, is a popular method of achieving stable levitation in an electric field. By employing changing potentials on four plates, charged particles can be trapped and stably levitated at the center of the trap[6].

Furthermore, optical levitation, achieved through optical tweezers, utilizes focused laser beams to hold and manipulate small dielectric particles. While optical tweezers themselves do not provide stable levitation, when particles are trapped without any support other than the laser beam, it can be considered as optical levitation. Optical levitation is advantageous for its ability to levitate objects in air or vacuum and offers attractive forces based on the relative refractive index between the particle and the surrounding medium[7]. The quality factor (Q-factor) of optical tweezers, which quantifies the trapping efficiency, depends on the trapping force, laser power, light velocity, and refractive index of the medium[8].

In addition to optical levitation, another method is acoustic levitation, which relies on high-intensity sound waves to levitate objects. Unlike other forms of levitation, acoustic levitation is independent of electrical charge, magnetic susceptibility, or refractive index. This technique allows for the suspension of both liquids and solids and exhibits stability in three-dimensional configurations. By manipulating the sound waves, objects can be controlled and moved within the levitation field[9].

Another approach to levitation involves diamagnetic materials, which are always repelled by a magnetic field. When a magnetic field is applied to a diamagnetic material, it induces a magnetic field in the opposite direction, resulting in a repellent force. This unique property, combined with an inhomogeneous magnetic field, enables stable and free levitation[5].

Table 1.1 shows a comparison of the pros and cons of the different levitation techniques discussed previously.

	Magnets	Superconductive	Diamagnetic	Electrostatic	Quadrupole ion trap	Optical	Acoustic
Passive levitation	✓	x	✓	x	x	x	x
Stable levitation without any stabilization technique	x	✓	✓	x	✓	x	x
Vacuum compatibility	✓	✓	✓	✓	✓	✓	x
Ability to levitate macro scale	✓	✓	✓	x	x	x	x
Ability to levitate any material	x	x	x	x	x	x	✓

Table 1.1: A comparison of the different levitation techniques.

The relation between the magnetization of a material $\mathbf{M}$ and the magnetic field strength $\mathbf{H}$ is defined as:

$$\mathbf{M} = \chi_v \mathbf{H}$$

From this, it can be seen that diamagnetic materials have a volume magnetic susceptibility (χ_v) less than or equal to 0 in order to create an opposing magnetic field compared to the magnetic field source. Superconductors, in particular, can be considered perfect diamagnets since they have a volume magnetic susceptibility of $\chi_v = -1$[10]. However, superconductors need to be kept at very low temperatures to exhibit their superconducting properties.

There are many materials that exhibit diamagnetic properties. Some notable examples include pyrolytic carbon, bismuth, neon, mercury, silver, carbon (diamond and graphite), lead, copper, and water.

Moreover, in recent years, significant advancements have been made in levitating various objects using diamagnetic materials and strong permanent magnets. Liquid droplets, cells, and solid particles have been successfully levitated using small permanent magnets, opening up possibilities for applications such as accelerometers, energy harvesters, viscosity and density sensors, and force sensors[11–14].

Additionally, pyrolytic graphite stands out as a particularly intriguing material for diamagnetic applications. It demonstrates robust diamagnetic properties at room temperature, as shown in Table 1.2[2].

Property	**Symbol**	**Value**	**Unit**
Density	ρ	2070	kg/m^3
Susceptibility $\perp$	χ_z	-450	$\times 10^{-6}$
Susceptibility $\parallel$	$\chi_{x,y}$	-85	$\times 10^{-6}$
Conductivity $\perp$	σ_z	200	S/m
Conductivity $\parallel$	$\sigma_{x,y}$	200000	S/m

Table 1.2: Properties of pyrolitic graphite[2].

These properties make pyrolytic graphite an ideal material for various applications involving diamagnetic levitation and sensing.

The quality factor is a dimensionless parameter that characterizes the damping and oscillatory behavior of a system. It is commonly used in physics and engineering to describe the quality or performance of resonant systems.

In the context of damping, energy dissipation occurs in a system, resulting in the decay of oscillations or vibrations. This phenomenon can be quantified by considering the amount of power dissipated by the eddy currents per unit mass for a thin sheet, as given by the following formula[15]:

$$P = \frac{\pi^2 B_p^2 d^2 f^2}{6\rho D} \tag{1.1}$$

A high Q factor indicates a low rate of energy dissipation and, consequently, a longer duration of oscillation or resonance. In contrast, a low Q factor implies a significant energy loss per cycle and faster damping of the oscillations.

Damping can arise from various sources, including air damping and eddy current damping. While air damping occurs when the motion of an object through air leads to the dissipation of energy, eddy current damping is another form of damping that occurs due to the generation of eddy currents in a conductor.

Air damping, for instance, occurs as the drag force exerted by the air on the object causes energy loss. However, in certain cases, this effect can be minimized or eliminated by operating the system in a vacuum. By reducing or removing the air molecules that interact with the system, the influence of air damping can be significantly reduced[2].

On the other hand, eddy current damping is specific to conductors. Eddy currents are induced by a changing magnetic field passing through the conductor. These circulating currents create their own magnetic field, which opposes the motion that induced them. Consequently, energy is dissipated as heat in the conductor, resulting in damping of the system.

Both air damping and eddy current damping contribute to the overall damping of a system and affect its Q factor. Minimizing or controlling these damping sources is important in designing systems with high Q factors and prolonged oscillations.

When utilizing diamagnetic levitation for applications such as accelerometers, energy harvesters, and sensors, minimizing damping becomes crucial in order to achieve a high Q factor[16]. Specifically, when levitating a pyrolytic graphite plate over magnets and inducing vibrations, the generation of eddy currents due to the magnetic flux change in the plate leads to drag forces and damping[16]. To mitigate the effects of eddy currents in the pyrolytic graphite plate, one approach is to reduce its size. Smaller plate sizes result in fewer eddy currents. However, this reduction in plate size also limits the size of objects that can be effectively levitated on the plate, such as droplets. To overcome this limitation, researchers have incorporated pyrolytic graphite micro-particles (powder) into an electric insulating composite. This composite hinders the free flow of eddy currents when the particles do not touch[16]. By employing this approach, a higher Q factor can be achieved. In experimental studies, a Q factor as high as 0.5 million was achieved by dispersing graphite powder with a particle size ranging from 2.7 to 22.7μm in Epotek 302-3M epoxy[16].

The measurement setup for these experiments involved an MSA400 Polytec laser Doppler vibrometer (LDV) for readout and the electrostatic excitation method. The levitating diamagnetic plate was driven into resonance using an actuation voltage generated by a function generator and amplified by a 20× voltage amplifier. The electrostatic force was generated by magnets connected to electrodes beneath the levitating plate, with insulation provided by Kapton tape. The MSA laser beam was focused on the plate to detect the vibration signal, and the acquired velocity was transferred to a PC for spectral analysis[16].

To quantify the damping effect of eddy currents on the levitating resonator, a finite element method (FEM) model was developed using COMSOL, a multiphysics simulation software[2]. The FEM model allowed for visualization of the distribution of eddy currents within the material. The model also predicted the Q factor as a function of plate length (L), with scaled plate thickness ($t = 0.03L$) and magnet size ($D = 1.2L$)[2].

When comparing the Q factor from the simulation to the Q factor measured with the pyrolytic graphite powder plate, it was observed that the measured Q factor was lower than the theoretical prediction for equal plate length. This discrepancy was attributed to the clustering of graphite micro-particles, which resulted in increased plate length and more eddy currents, leading to a lower Q factor.

Therefore, the critical research question that arises is:

How can the distribution of the graphite micro-particles be controlled and thus ensure that no micro-particles are making contact to reduce the eddy currents and therefore increase the quality factor without losing the ability to levitate macro-scale objects?

Furthermore, a secondary goal arising from the comprehensive research is:

the existing FEM model to quantify the eddy current damping should be verified.

The future goal is to increase the Q factor even further to a million or higher. The primary focus in achieving this goal lies in decreasing the presence of eddy currents in the pyrolytic graphite plate. Several approaches have been explored to realize this.

One option is to experiment with different outer shapes for the graphite plate, as it may slightly interrupt the path of the eddy currents. However, the majority of the eddy currents would still be able to move freely through the material. Another approach is to decrease the size of the graphite plate, which reduces the number of eddy currents[16]. However, this reduction in size would also result in the loss of the ability to levitate macro-scaled objects, which is an important property to maintain.

Introducing cuts in the graphite plate can effectively reduce eddy currents, but randomly placed cuts may not yield satisfactory results. One potential approach involves making cuts in locations where eddy currents are predicted to be dominant, based on a verified FEM (finite element method) model. Additionally, using a finer pyrolytic graphite powder than the one used in previous experiments has the potential to increase the Q factor[16]. However, producing a finer powder size than the current range of $2.7-22.7\mu m$ poses challenges. Furthermore, this approach does not address the issue of particle clustering mentioned earlier.

Using a different composite material than Epotek 302-3M epoxy to disperse the graphite powder could be an alternative. If the composite has a lower density than the epoxy, such as silica aerogel, less powder would be needed to achieve levitation. However, this change would not completely solve the clustering problem, although there would be reduced clustering due to the lower number of particles in an equal volume, assuming an equal particle distribution.

Another approach involves positioning the graphite powder particles in a controlled manner to ensure no clustering. However, achieving this level of control with a powder dispersion in a composite material seems challenging. Alternatively, using segmented pieces of solid pyrolytic graphite instead of a powder dispersion allows for accurate placement of segments, ensuring no contact between them. If the segments can be made small enough, it is possible to achieve very high Q factors.

Several techniques have been explored to create these segments, such as lithography and laser cutting. However, lithography methods like photolithography and electron-beam lithography are expensive and may not be suitable for pyrolytic graphite[17–19]. While atomic force microscopy (AFM)-based electrochemical etching has been investigated for lithography at the single atomic layer level in pyrolytic graphite[20], it appears to be less applicable for etching larger structures. In contrast, laser cutting offers a more cost-effective and accessible approach that can be implemented using the existing laser cutter available at the Delft University of Technology.

The initial results of the laser cutting experiments have shown an increase in the Q factor when the pyrolytic graphite plate is cut into segments. However, the increase is not as substantial as expected, likely due to the cuts not fully penetrating the graphite plate. This allowed eddy currents to pass between the segments, resulting in more eddy currents and a lower Q factor. In future experiments, addressing this issue by adjusting laser parameters or utilizing a different non-conductive base layer will be necessary.

Chapter 2

Paper

Enhancing the Q Factor of Diamagnetically Levitating Resonators by Segmentation

Eli Weisz
Delft University of Technology
Department of Precision and Microsystems Engineering
August 24, 2023

Abstract

Diamagnetic levitation presents a promising platform for realizing resonant sensors and energy harvesters. The technique offers mechanical isolation from the environment while operating with zero power consumption. This unique feature ensures exceptional sensitivity and accuracy in numerous applications. However, the presence of eddy currents in the levitating plate, induced by the alternating magnetic field, poses challenges, leading to increased damping and subsequently limiting the performance of levitating resonators. To address these issues, this study proposes a novel solution through the segmentation of diamagnetic plates. By dividing a pyrolytic graphite plate into smaller blocks, the flow of eddy currents is effectively restricted, resulting in reduced damping and significantly higher Q factors. By comparing the theoretical predictions using a FEM model from an earlier study with the measurements conducted the proposed technique is further validated. This comparative analysis demonstrates the effectiveness of the segmentation approach in mitigating damping due to eddy currents. Furthermore, the implementation of the proposed method led to remarkable results, with achieved Q factors exceeding 150 thousand.

Introduction

Levitation of micro- and nano-objects has captivated the scientific community due to its potential applications in various fields such as containerless processing[21,22], material investigation[22–24], frictionless bearings[25], spectroscopy[26,27], accelerometers[28,29], energy harvesters[30–32], viscosity/density sensors[33], and force sensors[14]. Researchers have explored different levitation techniques, including magnetic, electric, optical, and acoustic levitation[1]. Each technique offers unique advantages and has been instrumental in advancing the levitation technology.

When utilizing diamagnetic levitation for applications such as accelerometers, energy harvesters, and sensors, minimizing damping becomes crucial to achieve a high quality factor (Q factor)[16]. In particular, when levitating a pyrolytic graphite plate over magnets and inducing vibrations, the generation of eddy currents due to the magnetic flux change in the plate leads to drag forces and damping[16].

To mitigate the effects of eddy currents in pyrolytic graphite plates, one approach is to reduce their size, as smaller plates result in fewer eddy currents. However, this reduction in plate size imposes limitations on the size of objects that can be effectively levitated, such as droplets. To overcome this challenge, researchers have incorporated pyrolytic graphite micro-particles (powder) into an electric insulating composite, which impedes the free flow of eddy currents when the particles do not touch[16]. This approach has shown promise, with experimental studies achieving Q factors as high as 0.5 million by dispersing graphite powder with particle sizes ranging from 2.7 to 22.7μm in Epotek 302-3M epoxy[16].

However, the measured Q factor of the pyrolytic graphite powder plate was observed to be lower than the theoretical prediction for equal plate length due to the clustering of graphite micro-particles. This clustering increased the effective plate length and resulted in more eddy currents, leading to a lower Q factor. Therefore, the critical research question that arises is:

How can the distribution of graphite micro-particles be controlled to ensure that no micro-particles are in contact, thereby reducing eddy currents and increasing the quality factor without compromising the ability to levitate macro-scale objects?

Additionally, this comprehensive research aims to address a secondary goal:

To verify the existing finite element method (FEM) model used to quantify the eddy current damping.

In this paper, we present our experimental investigation into enhancing the Q factor of diamagnetically levitating resonators through segmentation. We propose a novel approach to control the distribution of graphite micro-particles, minimizing eddy currents while preserving the levitation capability for macro-scale objects. Furthermore, we verify the accuracy of the existing FEM model for quantifying eddy current damping.

The subsequent sections will detail our methodology, present the results of our experiments, discuss the findings, and conclude with the implications and future directions of this research.

Methodology

Sample Preparation

To conduct the experiment, we used pyrolytic graphite plates measuring $2 \times 2mm$. The sample preparation involved the following steps: laser cutting, epoxy application, and polishing.

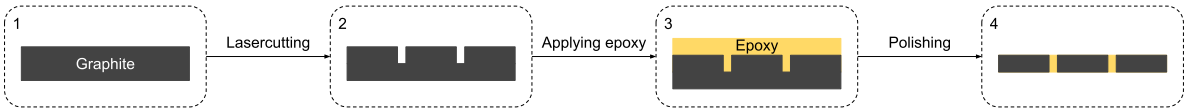

(a)

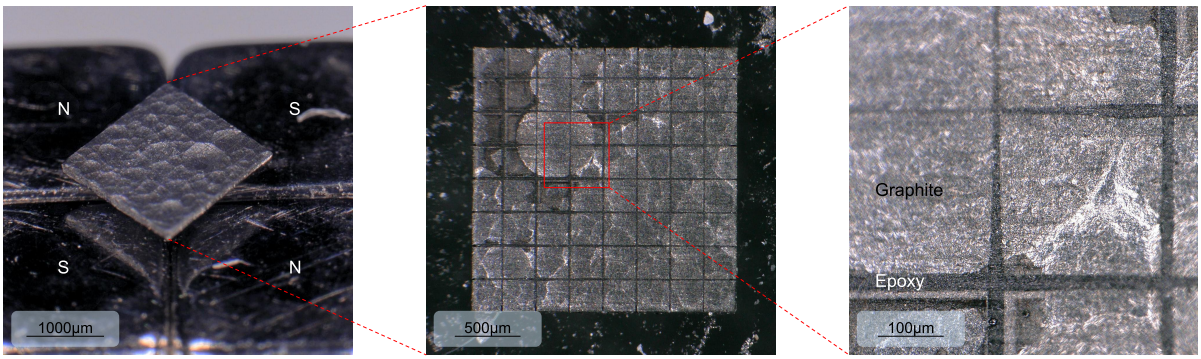

(b)

Figure 2.1: (a) Schematic of the sample preparation process: laser cutting, epoxy application, and polishing. (b) A segmented pyrolytic graphite plate featuring an 8×8 pattern, accompanied by zoomed-in images that highlight both the complete pattern and the segmentation.

Pyrolytic graphite plates were prepared through a series of well-defined steps to achieve the desired structure and properties.

The process began with a full pyrolytic graphite plate (Number 1), which served as the starting material (see Figure 2.1a). Using a precise LASEA laser cutter, horizontal and vertical lines were etched onto the graphite plate in a square pattern (Number 2). The laser-cut grooves were intentionally not entirely cut through the plate, in order to preserve its structural integrity. Subsequently, an essential step involved the careful application of epoxy resin into the laser-cut grooves (Number 3). This process firmly held each segment together, providing the much-needed structural stability for the plate.

In the next phase, a smaller $2 \times 2mm$ plate was cut from a larger plate of graphite, though this specific step was not depicted in the figure. This prepared plate then underwent a thorough polishing process on both the epoxy side and the graphite side. This polishing effectively eliminated any excess graphite material and residual epoxy, resulting in a smooth surface finish with clearly defined segments (Number 4).

Additionally, Figure 2.1b showcases an exemplary 8×8 segmented pyrolytic graphite plate, highlighting the successful application of the described segmentation process.

The prepared segmented pyrolytic graphite plates served as the basis for our investigation into the enhancement of the Q factor of diamagnetically levitating resonators. The next section presents the methodology employed to assess the impact of segmentation on the resonators' performance.

Experimental Setup

The measurement setup for this research consists of an MSA400 Polytec Laser Doppler Vibrometer (LDV) and an electrostatic excitation system, the latter being housed within a vacuum chamber. The vacuum chamber is utilized to minimize damping losses due to air resistance and maintain a controlled environment for accurate measurements. Figure 2.2a illustrates the measurement setup with the vacuum chamber.

The electrostatic excitation system includes a function generator that generates the actuation voltage. This voltage is then amplified by a 20× voltage amplifier, which drives the levitating plate into resonance. The levitating plate is positioned within the vacuum chamber and subjected to electrostatic forces transferred by magnets connected to electrodes. To ensure proper insulation and prevent any electrical interference, the magnets are separated by a layer of Kapton tape.

The MSA400 LDV, positioned outside the vacuum chamber, is utilized to measure the vibration of the levitating plate. It operates by focusing a laser beam onto the plate, detecting the Doppler shift of the reflected light. This enables precise and accurate measurements of the plate's velocity. The acquired velocity data is then transferred to a PC for spectral analysis.

The controlled environment within the vacuum chamber ensures that external factors are minimized, providing reliable data for the evaluation of the laser cutter segmentation's impact on reducing eddy currents.

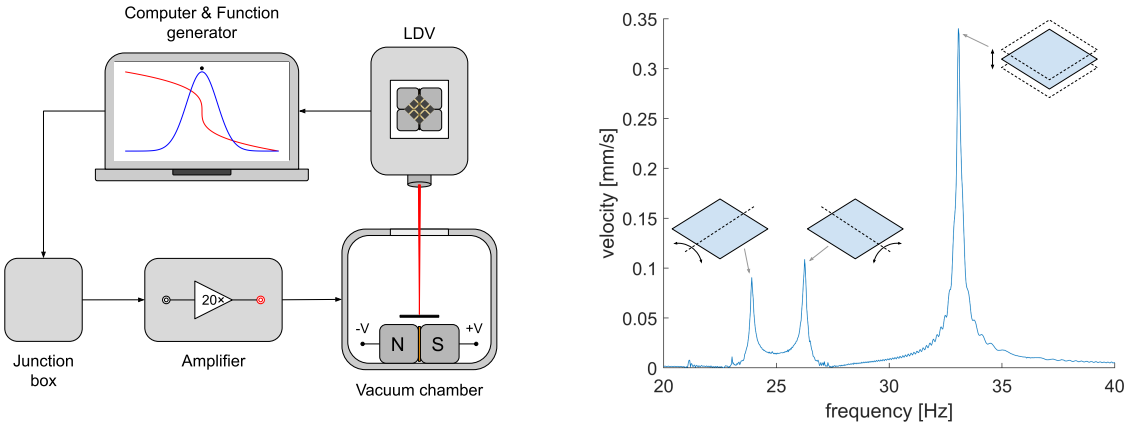

(a) (b)

Figure 2.2: (a) Measurement setup with the MSA400 Polytec LDV, the vacuum chamber, and the electrostatic excitation method. (b) Frequency response curve of the 8×8 pattern plate at $\approx 1mbar$. The observed mode shapes are shown schematically close to the corresponding resonance peaks.

Results

In this section, our focus lies on exploring the impact of segmentation on the Q factor of the resonators. To delve into this, we initiated an experiment that involved the measurement of the ringdown response of the levitating resonators. The purpose of this experiment is to gain insight into how segmentation affects the Q factor.

Before conducting the analysis of the free vibration decay, it is essential to determine the resonant frequencies of the system. This information is crucial for exciting the resonator into its resonant states during the subsequent measurements. The resonant frequencies are depicted in Figure 2.2b, showcasing the frequency response curve of the 8×8 pattern plate at an approximate pressure of $1mbar$. The curve exhibits distinct resonance peaks corresponding to specific modes of vibration. The first peak, situated around $24Hz$, signifies rotation about the x-axis, while the second peak, at roughly $26Hz$, corresponds to rotation about the y-axis. The third peak, occurring near $33Hz$, represents vertical movement along the z-axis. It is noteworthy that this third mode boasts the highest Q factor among all observed modes.

Within these primary peaks that denote the eigenmodes, smaller peaks emerge, indicating the presence of higher-order harmonics and sub-harmonics of these eigenmodes. However, the precision of the frequency response curve could have been influenced by the quality of the graphite plate's reflective surface. Imperfections in the reflective surface might have led to undesired reflections and noise, resulting in the appearance of supplementary minor peaks in the frequency response curve.

With the resonant frequencies identified, the subsequent step involves executing the free vibration decay measurement methodology. This technique entails exciting the resonator into a resonant state using electrostatic force and subsequently terminating the driving force to monitor the decay of the oscillations. The decay process can be suitably modeled using an exponential decay function $\propto e^{-t/\tau}$, where τ denotes the decay time.

In Figure 2.3a, an exemplar measurement is presented, illustrating the decay behavior of a 4×4 pattern plate featuring a graphite particle size of $490\mu m$ under a vacuum pressure of $1.2 \times 10^{-5}mbar$. The figure provides insight into the free oscillation decay curve of the resonator, accompanied by the fitted envelope. This comprehensive approach to characterizing the resonator's behavior aids in understanding its dynamic properties and behavior.

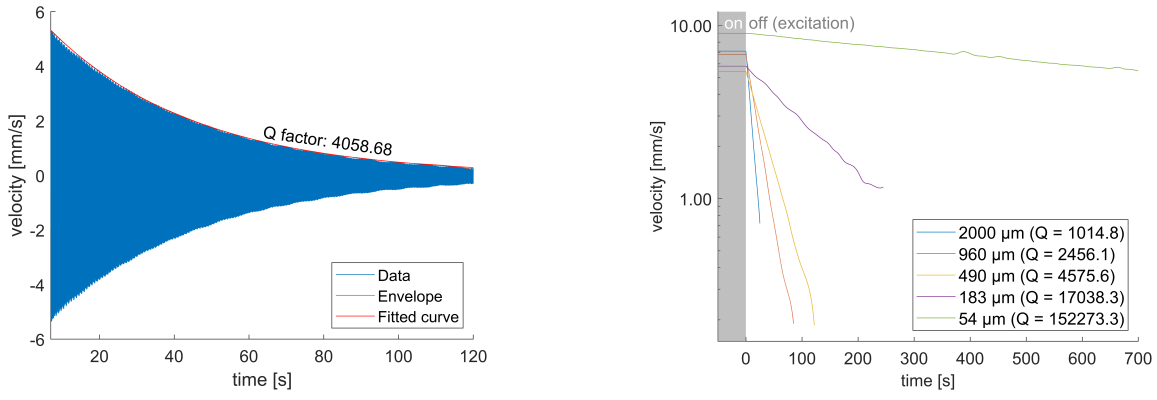

(a) (b)

Figure 2.3: (a) Free oscillation decay of a 4x4 pattern plate with a graphite particle size of $490\mu m$ at $1.2 \times 10^{-5}mbar$, along with the fitted envelope resulting in a Q factor of 4058.68. (b) Shows the decay for a full graphite plate and multiple other patterns.

Illustrated in Figure 2.3b are the results of multiple free vibration decay experiments. The experiments involved a levitating full graphite plate and five patterned plates, each with different particle sizes and patterns (2×2, 4×4, 8×8, and 32×32). The corresponding particle sizes were $960\mu m$, $490\mu m$, $183\mu m$, and $54\mu m$.

The measurements were conducted under vacuum conditions, with the vacuum pressure varying from $2.0 \times 10^{-5} mbar$ to $2.4 \times 10^{-6} mbar$. The pressure range is considered acceptable for analysis since, below $2.0 \times 10^{-5} mbar$, only the eddy currents impact the damping[16].

The most notable finding from the figure is that the plate with the smallest particle size (32×32 pattern with $54 \mu m$ particles) exhibited the highest Q factor among all the configurations tested, with a Q factor of $152,273.3$.

These results confirm the effectiveness of segmentation in enhancing the Q factor of diamagnetically levitating resonators. The smaller particle size and finer segmentation lead to reduced energy dissipation and improved resonator performance.

To delve into the intricate effects of segmentation on composite materials, it's essential to highlight the role of particle size. This study focuses on how particle size impacts levitation height, vibrational modes, and the Q factor within composite systems. Analyzing these relationships helps uncover how segmentation-induced changes in particle size affect how the pyrolytic graphite plates respond to forces, vibrations, and energy dissipation. In short, understanding particle size's impact enhances our comprehension of segmentation's influence on material behavior.

Depicting both experimental measurements and COMSOL simulations, the correlation between graphite particle size and levitation height is shown in Figure 2.4a. In the simulations, a constant plate thickness of $0.2mm$ was assumed. The results from the simulations reveal that decreasing particle size leads to a reduction in levitation height. This effect stems from the decrease in graphite volume fraction within the composite material. Smaller particles translate to less diamagnetic material, resulting in a weaker repulsive force against gravity.

Nevertheless, the observed levitation heights for various particle sizes lack a distinct pattern. This discrepancy likely arises from inconsistencies in graphite and epoxy thickness among the samples. These thickness variations introduce irregularities in the levitation behavior, hindering the establishment of a direct link between particle size and levitation height based solely on experimental observations.

Moving on to Figure 2.4b, the figure portrays the connection between graphite particle size and resonant frequency for the third vibration mode, depicted in Figure 2.2b. Both simulation and measurement data are depicted. This third mode showcases the plate's up-and-down motion and was chosen specifically for vibration decay measurements.

The simulation data demonstrates that diminishing particle size corresponds to an increase in the resonant frequency. This shift originates from alterations in graphite and epoxy volume fractions within the composite material. As particle size decreases, the graphite fraction diminishes while the epoxy fraction rises. Considering pyrolytic graphite's density $(2070 kg/m^3)$[2] and epoxy's density $(1150 kg/m^3)$[34,35], the plate's total mass drops. In a spring-mass system, mass and frequency are inversely proportional, leading to higher resonant frequency with smaller particle sizes. This connection can be expressed as $f \propto \frac{1}{\sqrt{m}}$, where f represents frequency and m symbolizes mass.

However, the resonant frequencies observed for diverse particle sizes lack a clear trend. This absence of a logical pattern can be attributed to discrepancies in graphite and epoxy thicknesses among different samples. These variations introduce deviations in resonant behavior, making it challenging to establish a straightforward relationship between particle size and resonant frequency solely based on experimental findings.

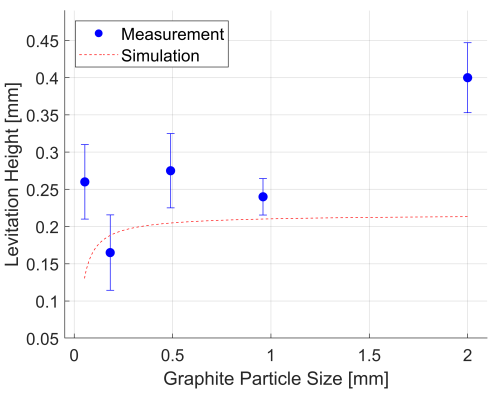

(a)

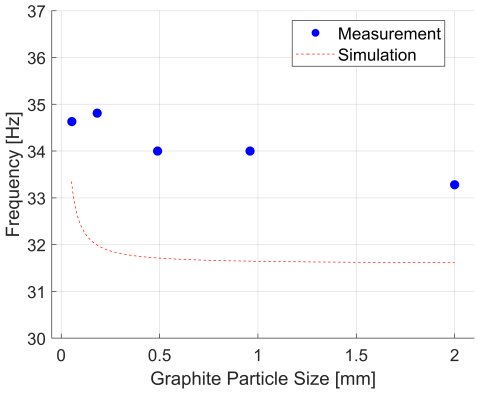

(b)

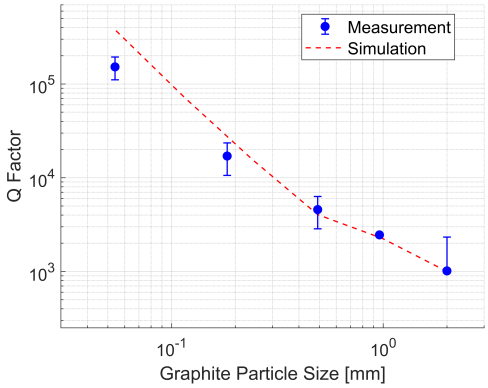

(c)

Figure 2.4: (a) Graphite particle size vs. levitation height for experimental measurements and COMSOL simulations. The simulation data reveals a decreasing levitation height trend as particle size decreases due to the reduction in the volume fraction of graphite. The measured levitation heights for different particle sizes show no clear trend, likely due to varying graphite and epoxy thicknesses in the samples. (b) Graphite particle size vs. resonant frequency for the third mode of vibration. The simulation data demonstrates an increasing trend of resonant frequency as particle size decreases due to changes in the volume fraction of graphite and epoxy, resulting in a decrease in the total plate mass. The measured resonant frequencies for the third mode do not exhibit a clear trend, likely due to varying graphite and epoxy thicknesses in the samples. (c) Graphite particle size vs. Q factor for simulation and measurement data. Both datasets exhibit a clear trend: as the particle size decreases, the Q factor increases. The measured Q factors deviate slightly lower than the simulation data, possibly due to imperfections in the experimental setup and sample preparation, such as incomplete separation of segmented blocks or the presence of graphite powder in the epoxy.

Lastly, in Figure 2.4c, the depiction outlines the relationship between graphite particle size and Q factor, considering both simulation and measurement data. Both datasets exhibit a consistent pattern: decreasing particle size corresponds to an increase in Q factor, mirroring the observations in Figure 2.3b. The simulation and measured data closely align, with Q factors closely matching for most particle sizes.

However, as particle size decreases further, the measured Q factor slightly deviates, falling below the simulation data. This divergence can be attributed to imperfections in the experimental setup and sample preparation. Factors such as incomplete separation of segmented blocks or the presence of graphite powder in the epoxy due to the laser cutting process may contribute to the lower measured Q factors.

The integration of a finite element method (FEM) model, for this study a COMSOL model, is pivotal in decoding the relationship between eddy current density and segmentation effects. These simulations provide a dynamic platform to visualize and quantify eddy current behavior under various segmentation patterns. By directly observing eddy current density distributions in Figure 2.5, we bridge theory and observation, offering quantitative insights into how segmentation influences eddy currents. This modeling approach enables us to establish a quantitative foundation for subsequent analyses, connecting eddy currents to damping coefficients and the Q factor. In essence, COMSOL simulations enhance our understanding of how particle size and segmentation intricately shape material responses.

In Figure 2.5, we can observe the distribution of eddy current density obtained from COMSOL simulations for different patterns: a full graphite plate, a 16×16 pattern, and a 32×32 pattern. The eddy current density is represented using color maps, where warmer colors indicate higher densities.

The first image, Figure 2.5a, illustrates the full graphite plate, showing a relatively uniform and high eddy current density across the entire plate. As we reduce the particle size in the pattern, the eddy current density decreases. This trend is evident in both the 16×16 pattern (Figure 2.5b) and the 32×32 pattern (Figure 2.5c). In these segmented patterns, the eddy current density becomes more localized within the individual segments above the corners of the magnets, resulting in a significant reduction in overall density compared to the full plate.

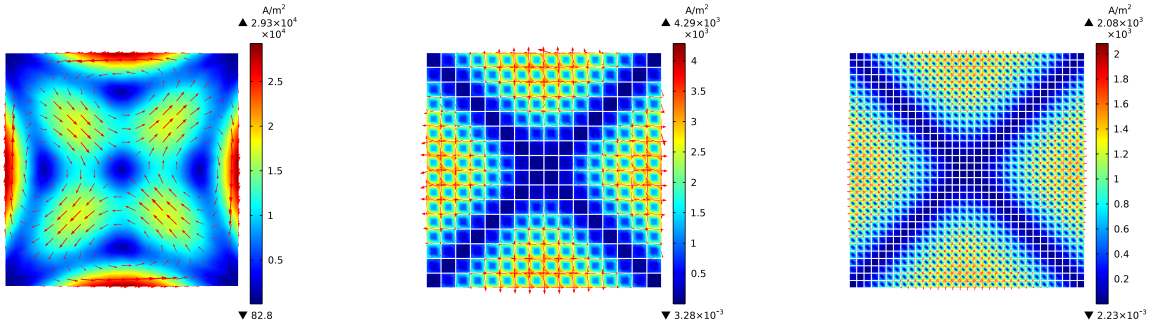

(a) Full Graphite Plate (b) 16×16 Pattern (c) 32×32 Pattern

Figure 2.5: Eddy current density distribution from COMSOL simulation for different patterns: (a) Full Graphite Plate, (b) 16×16 Pattern, (c) 32×32. The eddy current density decreases as the particle size is decreased.

Now, let's explore the relationship between the eddy current density and the Q factor. We calculate the force exerted by the eddy currents, represented as $\mathbf{F_e}$, using the equation:

$$\mathbf{F_e} = \int_V (\mathbf{J} \times \mathbf{B}) dV \tag{2.1}$$

Here, $\mathbf{J}$ denotes the eddy current density vector, and $\mathbf{B}$ represents the magnetic flux density vector. Since the plate's velocity is assumed to be only in the z-direction, we can relate the force $\mathbf{F_e}$ to the damping coefficient c and the velocity $\mathbf{v}$ through the equation:

$$\mathbf{F_e} = -c\mathbf{v} \tag{2.2}$$

Furthermore, the Q factor of the system, denoted as Q, can be related to the plate's mass m and its resonant frequency f_{res} using the equation:

$$Q = \frac{2\pi m f_{\text{res}}}{c} \tag{2.3}$$

In Table 2.1 the values of the damping coefficient and Q factor for the three patterns are shown, considering: The velocity of the plate is assumed to be $1m/s$. The mass of the plate is assumed to be $1.66 \times 10^{-6}kg$. The resonant frequency of the system is assumed to be $34Hz$.

Table 2.1: Values of c and Q for the three patterns.

Pattern	c	Q
Full Plate	3.54×10^{-7}	1000.40
16×16 Pattern	4.92×10^{-9}	71945.37
32×32 Pattern	8.77×10^{-10}	403610.51

Therefore, as we observe a decrease in the eddy current density due to segmentation, the force exerted by the eddy currents also decreases, leading to a reduction in the damping coefficient c. As a consequence, the Q factor of the system increases, indicating a higher quality factor and lower damping effects caused by eddy currents. The division of the plate into smaller segments restricts the flow of eddy currents, resulting in more efficient mitigation of damping effects and an overall improvement in the system's performance.

Discussion & Conclusion

The presented study explores the remarkable potential of segmented pyrolytic graphite plates in enhancing the Q factor of diamagnetically levitating resonators. An innovative approach was achieved to restrict eddy current flow, leading to reduced damping and substantially higher Q factors. This achievement holds significant promise for applications in accelerometers[28,29], energy harvesters[30–32], viscosity/density sensors[33], and force sensors[14].

By segmenting the graphite plate, eddy current density was successfully controlled, and minimized their detrimental effects on the resonators' performance. This strategic solution effectively addresses the challenge of damping, enhancing the Q factor, and enabling the realization of highly efficient levitating resonators.

While the results demonstrate considerable success, several limitations deserve attention. Variations in sample preparation, such as inconsistent epoxy distribution or variations in graphite and epoxy thickness, may contribute to the observed deviations in measurements. This aspect underscores the importance of refining the segmentation technique for consistent and repeatable results.

Looking ahead, further research is warranted to refine the segmentation process and mitigate limitations. Exploring advanced fabrication techniques, precise epoxy application methods, and improved polishing approaches could yield more consistent results and elevate the Q factor even further.

Additionally, investigating the integration of segmented pyrolytic graphite plates in practical applications remains an exciting avenue. Further studies could examine the impact of segmented designs on device performance, considering aspects like levitation stability, response time, and sensitivity.

In conclusion, this study unveils the potential of segmented pyrolytic graphite plates as a transformative solution for enhancing the Q factor of diamagnetically levitating resonators. While challenges persist, the demonstrated successes and future research directions promise to reshape the landscape of precision engineering and microsystems, opening new horizons for resonant sensors and energy harvesters.

Chapter 3

Conclusion & Reflection

This research explored the challenge of controlling graphite particle distribution to reduce eddy currents, enhance the quality factor, and keep the ability to levitate large objects intact. This section summarizes our findings, highlights their importance, acknowledges limitations, and suggests future research directions.

As mentioned in the beginning, our main question was: "How can the distribution of graphite micro-particles be controlled to ensure that no micro-particles are in contact, thereby reducing eddy currents and increasing the quality factor without compromising the ability to levitate macro-scale objects?" By carefully conducting experiments, analyzing data, and using computer models, we delved into the relationship between particle size and eddy currents.

Among the different patterns and particle sizes we tested, the plate with the smallest particles (32×32 pattern with $54\mu m$ particles) performed the best, showing a high Q factor of $152,273.3$. This emphasizes the role of particle size and distribution in improving the quality factor of diamagnetically levitating objects. When particle size decreases, eddy currents decrease too, showing that better performance can be achieved with finer particle size.

We also looked into how the size of graphite particles affects levitation height, using both experiments and simulations. However, variations in the thickness of graphite and epoxy in different samples made this relationship complex.

The simulations showed that smaller particles lead to higher resonant frequency. This happens because of changes in the composite mass. Although the experimental data didn't always show a clear pattern, this observation gives us a clue about the connection between particle size, resonant frequency, and diamagnetic levitation.

We observed a consistent trend when comparing simulation and measurement data for the Q factor in relation to particle size. As expected based on previous research and theoretical understanding, a reduction in particle size corresponded to an increase in the Q factor. This reaffirms our primary objective – the precise control of particle distribution leads to an enhancement in the quality factor of diamagnetic resonators.

This research goes beyond just levitation. The new method we introduced for controlling particle distribution using laser cutting has broad implications. It not only helps with reducing eddy currents but also validates models for eddy currents. This connection between theory and practice is a significant step forward.

This research journey is not without its limitations. Despite the valuable insights gained, certain challenges and limitations should be acknowledged. The practical execution of the theoretical idea proved intricate, especially as particle sizes diminished. Achieving optimal cutting parameters, a process that extended over weeks to months, occasionally posed demotivating hurdles. The inherent imperfections in the initial pyrolytic graphite plates, varying in thickness and surface quality, introduced unavoidable irregularities. Additionally, the process of epoxy deposition encountered difficulties in ensuring uniform distribution over the laser-cut graphite plate. The post-processing phase presented challenges due to

the small plate size, resulting in uneven pressure during polishing and potential discrepancies in particle distribution. The laser cutting process itself, as particles decreased in size, posed challenges in avoiding damage. Despite these limitations, each hurdle surmounted added to the depth of knowledge gained and the robustness of the conclusions drawn from this research.

Looking ahead, our research suggests several promising avenues for future exploration. One notable recommendation involves enhancing the quality of the initial graphite plates. Ensuring a uniform thickness and addressing any surface imperfections in these plates could significantly enhance the reproducibility and reliability of experimental results. Furthermore, a more precise deposition of epoxy onto the laser-cut graphite plate is recommended. Achieving a consistent distribution across the surface would contribute to the overall success of the approach.

In addition to these refinements, we propose a broader exploration of particle shapes and plate designs. Specifically, investigating alternative shapes for segmented particles and considering variations in the design of the levitating plate holds the potential to yield valuable insights. This is particularly relevant in regions where strong eddy currents are prevalent. By strategically placing smaller particles in these high-current zones, we may uncover new strategies for reducing eddy currents.

This research's significance extends beyond levitation; it impacts materials engineering too. Precisely controlling micro-particle distribution opens doors to composite material innovations that could shape industries from levitation to manufacturing.

Moreover, this study bridges theory and practice. By linking theoretical models with real-world measurements, it connects abstract ideas to practical solutions.

Reflecting on the journey of this research, it's clear that the theoretical framework laid out the path, but execution posed significant challenges, particularly as particle sizes decreased. Striving for optimal cutting parameters, a process that could take weeks to even months, at times cast a shadow of demotivation. Yet, through these challenges, an invaluable learning experience unfolded. This journey illuminated the essence of thorough and relevant research – from immersing oneself in relevant subject matter, identifying research gaps, and formulating precise research questions to devising and refining the optimal approach.

The practical process brought frequent returns to the drawing board, a reminder that unforeseen hurdles are an inherent part of groundbreaking research. This journey instilled the importance of resilience, adaptability, and unwavering dedication in overcoming obstacles and driving toward meaningful outcomes.

As we conclude this phase of research, we stand at the crossroads of newfound knowledge and unexplored possibilities. The insights gained will continue to shape our exploration, not only in levitation but also in various scientific avenues.

The lessons learned, challenges faced, and insights gained showcase the strength of scientific inquiry. We're grateful to all who contributed and look forward to seeing the impact of this research ripple across disciplines, sparking new ideas and shaping the trajectory of diamagnetically levitating resonators' evolution.

References

[1] E. H. Brandt. "Levitation in Physics". In: *Science* 243.4889 (1989), pp. 349–355. DOI: 10.1126/science.243.4889.349. eprint: https://www.science.org/doi/pdf/10.1126/science.243.4889.349. URL: https://www.science.org/doi/abs/10.1126/science.243.4889.349.

[2] Xianfeng Chen et al. "Rigid body dynamics of diamagnetically levitating graphite resonators". In: *Applied Physics Letters* 116 (24 June 2020). ISSN: 00036951. DOI: 10.1063/5.0009604.

[3] S. Earnshaw. "On the Nature of the Molecular Forces which Regulate the Constitution of the Luminiferous Ether". In: *Transactions of the Cambridge Philosophical Society* 7 (Jan. 1848), p. 97.

[4] Taha H Ababou. "Evolution of transportation systems with quantum levitation". In: ().

[5] Gerald Küstler. *Électrotechnique et électroénergétique DIAMAGNETIC LEVITATION-HISTORICAL MILESTONES*. 2007, pp. 265–282.

[6] Arian Kriesch Akriesch. *Paul-Trap*. [Online; accessed 15-August-2022]. 2006. URL: https://en.wikipedia.org/wiki/File:Paul-Trap.svg.

[7] A. Ashkin et al. "Observation of a single-beam gradient force optical trap for dielectric particles". In: *Opt. Lett.* 11.5 (May 1986), pp. 288–290. DOI: 10.1364/OL.11.000288. URL: http://opg.optica.org/ol/abstract.cfm?URI=ol-11-5-288.

[8] A. Ashkin. "Forces of a single-beam gradient laser trap on a dielectric sphere in the ray optics regime". In: *Biophysical Journal* 61.2 (1992), pp. 569–582. ISSN: 0006-3495. DOI: https://doi.org/10.1016/S0006-3495(92)81860-X. URL: https://www.sciencedirect.com/science/article/pii/S000634959281860X.

[9] Marco A. B. Andrade, Asier Marzo, and Julio C. Adamowski. "Acoustic levitation in mid-air: Recent advances, challenges, and future perspectives". In: *Applied Physics Letters* 116.25 (2020), p. 250501. DOI: 10.1063/5.0012660. eprint: https://doi.org/10.1063/5.0012660. URL: https://doi.org/10.1063/5.0012660.

[10] Carl L Nave. *Magnetic Properties of Solids. HyperPhysics*. Tech. rep. Retrieved 2008-11-09, 2008.

[11] Igor Lyuksyutov, D. Naugle, and K. Rathnayaka. "On-chip manipulation of levitated femtodroplets". In: *Applied Physics Letters* 85 (Oct. 2004), pp. 1817–1819. DOI: 10.1063/1.1781735.

[12] Hichem Chetouani et al. "Diamagnetic Levitation With Permanent Magnets for Contactless Guiding and Trapping of Microdroplets and Particles in Air and Liquids". In: *Magnetics, IEEE Transactions on* 42 (Nov. 2006), pp. 3557–3559. DOI: 10.1109/TMAG.2006.880921.

[13] Hichem Chetouani et al. "Diamagnetic Levitation of Beads and Cells Above Permanent Magnets". In: *Proceedings of the 14th International Conference on Solid-State Sensors, Actuators and Microsystems (Transducers & Eurosensors '07)* (June 2007). DOI: 10.1109/SENSOR.2007.4300230.

[14] M. Boukallel, J. Abadie, and E. Piat. "Levitated micro-nano force sensor using diamagnetic materials". In: *2003 IEEE International Conference on Robotics and Automation (Cat. No.03CH37422)*. Vol. 3. 2003, pp. 3219–3224. DOI: 10.1109/ROBOT.2003.1242086.

[15] Fausto Fiorillo. *Characterization and measurement of Magnetic Materials*. Elsevier Series in Electromagnetism. Elsevier Academic Press, 2004, p. 31.

[16] Xianfeng Chen et al. “Diamagnetic composites for high-Q levitating resonators”. In: (Aug. 2022).

[17] I. Tiginyanu, V. Ursaki, and V. Popa. “10 - Nanoimprint lithography (NIL) and related techniques for electronics applications”. In: *Nanocoatings and Ultra-Thin Films*. Ed. by Abdel Salam Hamdy Makhlouf and Ion Tiginyanu. Woodhead Publishing Series in Metals and Surface Engineering. Woodhead Publishing, 2011, pp. 280–329. ISBN: 978-1-84569-812-6. DOI: https://doi.org/10.1533/9780857094902.2.280. URL: https://www.sciencedirect.com/science/article/pii/B9781845698126500105.

[18] M. Van Rossum. “Integrated Circuits”. In: *Encyclopedia of Condensed Matter Physics*. Ed. by Franco Bassani, Gerald L. Liedl, and Peter Wyder. Oxford: Elsevier, 2005, pp. 394–403. ISBN: 978-0-12-369401-0. DOI: https://doi.org/10.1016/B0-12-369401-9/00503-9. URL: https://www.sciencedirect.com/science/article/pii/B0123694019005039.

[19] Richard A. Lawson and Alex P.G. Robinson. “Chapter 1 - Overview of materials and processes for lithography”. In: *Materials and Processes for Next Generation Lithography*. Ed. by Alex Robinson and Richard Lawson. Vol. 11. Frontiers of Nanoscience. Elsevier, 2016, pp. 1–90. DOI: https://doi.org/10.1016/B978-0-08-100354-1.00001-6. URL: https://www.sciencedirect.com/science/article/pii/B9780081003541000016.

[20] Wei Han et al. “Toward Single-Atomic-Layer Lithography on Highly Oriented Pyrolytic Graphite Surfaces Using AFM-Based Electrochemical Etching”. In: *Nanomanufacturing and Metrology* 5.1 (Mar. 2022), pp. 32–38. ISSN: 2520-8128. DOI: 10.1007/s41871-022-00127-9. URL: https://doi.org/10.1007/s41871-022-00127-9.

[21] Hui-Meng Lu et al. “A containerless levitation setup for liquid processing in a superconducting magnet”. In: *Review of Scientific Instruments* 79.9 (Sept. 2008), p. 093903. ISSN: 0034-6748. DOI: 10.1063/1.2980383. eprint: https://pubs.aip.org/aip/rsi/article-pdf/doi/10.1063/1.2980383/14867656/093903_1_online.pdf. URL: https://doi.org/10.1063/1.2980383.

[22] J.K.R. Weber et al. “Acoustic levitation: Recent developments and emerging opportunities in biomaterials research”. In: *European biophysics journal : EBJ* 41 (Oct. 2011), pp. 397–403. DOI: 10.1007/s00249-011-0767-3.

[23] Paul-François Paradis et al. “Materials properties measurements and particle beam interactions studies using electrostatic levitation”. In: *Materials Science and Engineering: R: Reports* 76 (2014), pp. 1–53. ISSN: 0927-796X. DOI: https://doi.org/10.1016/j.mser.2013.12.001. URL: https://www.sciencedirect.com/science/article/pii/S0927796X13001459.

[24] A Seidel, W Soellner, and C Stenzel. “Materials science investigations using electromagnetic levitation”. In: *Journal of Physics: Conference Series* 327.1 (Dec. 2011), p. 012015. DOI: 10.1088/1742-6596/327/1/012015. URL: https://dx.doi.org/10.1088/1742-6596/327/1/012015.

[25] Takeshi Ide et al. “A non-contact linear bearing and actuator via ultrasonic levitation”. In: *Sensors and Actuators A: Physical* 135.2 (2007), pp. 740–747. ISSN: 0924-4247. DOI: https://doi.org/10.1016/j.sna.2006.08.005. URL: https://www.sciencedirect.com/science/article/pii/S092442470600536X.

[26] Ljiljana Puskar et al. “Raman acoustic levitation spectroscopy of red blood cells and Plasmodium falciparum trophozoites”. In: *Lab Chip* 7 (9 2007), pp. 1125–1131. DOI: 10.1039/B706997A. URL: http://dx.doi.org/10.1039/B706997A.

[27] Rudolf Tuckermann et al. “Chemical analysis of acoustically levitated drops by Raman spectroscopy”. In: *Analytical and bioanalytical chemistry* 394 (June 2009), pp. 1433–41. DOI: 10.1007/s00216-009-2800-2.

[28] David Garmire et al. “Diamagnetically Levitated MEMS Accelerometers”. In: July 2007, pp. 1203–1206. DOI: 10.1109/SENSOR.2007.4300352.

[29] Christian Pigot, Benoit Delinchant, and Gilbert Reyne. "Optimization of a 3D micro-accelerometer based on diamagnetic levitation". In: *International Journal of Applied Electromagnetics and Mechanics* 30 (Sept. 2009), pp. 179–188. DOI: 10.3233/JAE-2009-1020.

[30] L. Liu and F. G. Yuan. "Nonlinear vibration energy harvester using diamagnetic levitation". In: *Applied Physics Letters* 98.20 (2011), p. 203507. DOI: 10.1063/1.3583675. eprint: https://doi.org/10.1063/1.3583675. URL: https://doi.org/10.1063/1.3583675.

[31] Lei Liu and Fuh-Gwo Yuan. "Diamagnetic levitation for nonlinear vibration energy harvesting: Theoretical modeling and analysis". In: *Journal of Sound and Vibration* 332 (Jan. 2013), pp. 455–464. DOI: 10.1016/j.jsv.2012.08.004.

[32] Sri Vikram Palagummi and Fuh-Gwo Yuan. "A bi-stable horizontal diamagnetic levitation based low frequency vibration energy harvester". In: *Sensors and Actuators A Physical* 279 (July 2018), pp. 743–752. DOI: 10.1016/j.sna.2018.07.001.

[33] Stefan Clara et al. "An advanced viscosity and density sensor based on diamagnetically stabilized levitation". In: *Sensors and Actuators A: Physical* 248 (July 2016), pp. 46–53. DOI: 10.1016/j.sna.2016.07.021.

[34] *Safety Data Sheet for YACHTCARE SUPER EPOXY (base)*. Electronic document. Accessed on August 18, 2023. 2023. URL: https://www.vosschemie-benelux.com/execute.php?page=downloadFile&isAppendix=true&id=2392.

[35] *Safety Data Sheet for YACHTCARE SUPER EPOXY (hardener)*. Electronic document. Accessed on August 18, 2023. 2023. URL: https://www.vosschemie-benelux.com/execute.php?page=downloadFile&isAppendix=true&id=2390.

Appendix A

MATLAB code Figure 2.2b

```
clear
close all
clc

% Set font size
font_size = 13;

% Import data
d = importdata('FFT.txt');
time = d.data(:, 1);
data = d.data(:, 2);

% Set start and end time (in seconds)
start_time = 0;    % Start time
end_time = 0;    % End time

% Filter data based on the specified time range
if start_time == 0 && end_time == 0
    % Use all data
    d_filtered = d.data;
else
    % Filter data based on the specified time range
    idx = (time >= start_time) & (time <= end_time);
    d_filtered = d.data(idx, :);
end

% Plot original data within the specified time range
figure(1);
% plot(time(idx), data(idx));
hold on

% Compute envelope
[up, lo] = envelope(d_filtered(:, 2), 2000, 'peak');

% Plot filtered data
plot(d_filtered(:, 1), d_filtered(:, 2));
yticklabels(get(gca, 'ytick') * 1000);
```

```
xlabel('frequency [Hz]', 'FontSize', font_size);
ylabel('velocity [mm/s]', 'FontSize', font_size);
set(gca, 'FontSize', font_size); % Set font size for tick labels and
    axis labels
grid off;
hold off;

%% If data is in the time domain

% Perform FFT on the filtered data
Fs = 1 / (time(2) - time(1));   % Sampling frequency
N = length(d_filtered(:, 2));   % Length of signal
fft_signal = fft(d_filtered(:, 2), N) / N;   % Compute FFT
frequencies = Fs * (0:(N/2)) / N;   % Frequency vector

% Plot the single-sided amplitude spectrum
figure(2);
plot(frequencies, 2 * abs(fft_signal(1:N/2+1)));
xlabel('Frequency [Hz]', 'FontSize', font_size);
ylabel('Amplitude', 'FontSize', font_size);
set(gca, 'FontSize', font_size); % Set font size for tick labels and
    axis labels
grid on;
```

Appendix B

MATLAB code Figure 2.3a

```
clear
close all
clc

% Import data
d = importdata('file.txt');
time = d.data(:, 1);
data = d.data(:, 2);

% Set measured resonant frequency
f0 = 33.25;

% Set start and end time (in seconds)
start_time = 7;     % Start time
end_time = 120;     % End time

% Filter data based on the specified time range
if start_time == 0 && end_time == 0
    % Use all data
    d_filtered = d.data;
else
    % Filter data based on the specified time range
    idx = (time >= start_time) & (time <= end_time);
    d_filtered = d.data(idx, :);
end

% Plot original data within the specified time range
figure(1);
% plot(time(idx), data(idx));
hold on

% Compute envelope
[up, lo] = envelope(d_filtered(:, 2), 2000, 'peak');

% Plot filtered data
plot(d_filtered(:, 1), d_filtered(:, 2));

```

```
% Plot envelope
plot(d_filtered(:, 1), up, 'DisplayName', 'Envelope')

% Fitting simple harmonic oscillator
fo = fitoptions('Method', 'NonlinearLeastSquares',...
                'Robust', 'Off',...
                'Algorithm', 'Trust-Region',...
                'DiffMinChange', 1.0e-8,...
                'DiffMaxChange', 0.1,...
                'MaxFunEvals', 600,...
                'MaxIter', 400,...
                'TolFun', 1.0e-9,...
                'TolX', 1.0e-6,...
                'Lower', [0, -1],...
                'Upper', [1, 0],...
                'StartPoint', [0.0006, -0.002]);
ft = fittype('A0 * exp(B0 * x)', 'options', fo);
[curve2, gof2, output2] = fit(d_filtered(:, 1), up, ft);

font_size = 13;

% Plot fitted curve
plot(curve2);
yticklabels(get(gca, 'ytick') * 1000);
xlabel('time [s]', 'FontSize', font_size);
ylabel('velocity [mm/s]', 'FontSize', font_size);
set(gca, 'FontSize', font_size); % Increase tick label font size
xlim([start_time, end_time])
grid off
hold off

% Compute parameters
Tao = -1 / curve2.B0;
A0_fitted = curve2.A0;
B0_fitted = curve2.B0;
Rsquare = gof2.rsquare;
Q = pi * f0 * Tao;

% Display Q factor
fprintf('Q factor: %.2f\n', Q);

% Add Q factor to figure 1
figure(1);
legend('Data', 'Envelope', 'Fitted curve', 'Location', 'southeast', '
    FontSize', 12);
% Find the middle point of the fitted curve
middle_point = (min(d_filtered(:, 1)) + max(d_filtered(:, 1))) / 2;
middle_velocity = feval(curve2, middle_point);
text(middle_point, middle_velocity, sprintf('Q factor: %.2f', Q), '
    HorizontalAlignment', 'left', 'FontSize', font_size, '
    VerticalAlignment', 'bottom', 'Rotation', -8);
```

Appendix C

MATLAB code Figure 2.3b

```
clear
close all
clc

% Define font size
font_size = 13;

% File names
fileNames = {'d_filtered_1x1.mat', 'd_filtered_2x2.mat', 'd_filtered_4x4.mat', 'd_filtered_8x8.mat', 'd_filtered_32x32.mat'};

% Set axis limits
xmin = -50;
xmax = 700;
ymin = 0.00015;
ymax = 0.012;

figure;
hold on;

colors = lines(numel(fileNames)); % Generate a color matrix for different lines

x_data = cell(numel(fileNames), 1); % Cell array to store 'x' data from each iteration
up_data = cell(numel(fileNames), 1); % Cell array to store 'up' data from each iteration

for i = 1:numel(fileNames)
    % Import data
    data = importdata(fileNames{i});

    % Shift x-axis to start from 0
    x = data(:, 1) - data(1, 1);

    % Compute envelope
    [up, lo] = envelope(data(:, 2), 2000, 'peak');
```

```
34
35      % Plot envelope using plot
36      plot(x, up, 'DisplayName', ['Envelope ', num2str(i)], 'Color',
            colors(i, :));
37
38      % Store 'x' and 'up' data
39      x_data{i} = x;
40      up_data{i} = up;
41  end
42
43  % Extend the lines horizontally to xmin
44  for i = 1:numel(fileNames)
45      x = x_data{i};
46      up = up_data{i};
47      line([xmin, x(1)], [up(1), up(1)], 'Color', colors(i, :), 'LineStyle
            ', '-');
48  end
49
50  hold off; % Disable the hold state
51
52  % Add opaque grey color patch
53  patch([0 xmin xmin 0], [ymin ymin ymax ymax], [0.5 0.5 0.5], 'FaceAlpha'
        , 0.5, 'EdgeColor', 'none');
54
55  % Adjust the axis limits
56  xlim([xmin, xmax]);
57  ylim([ymin, ymax]);
58
59  % Set y-axis to logarithmic scale
60  set(gca, 'YScale', 'log');
61
62  % Edit y-axis tick labels
63  yticks(get(gca, 'ytick'));
64  yticklabels(arrayfun(@(x) sprintf('%.2f', x * 1000), get(gca, 'ytick'),
        'UniformOutput', false));
65
66  % Set font size for tick labels
67  set(gca, 'FontSize', font_size);
68
69  % Add 'on' text label
70  text(-5, ymax, 'on', 'Color', 'white', 'HorizontalAlignment', 'right', '
        VerticalAlignment', 'top', 'FontSize', font_size);
71
72  % Add 'off' text label
73  text(5, ymax, 'off (excitation)', 'Color', [0.5 0.5 0.5], '
        HorizontalAlignment', 'left', 'VerticalAlignment', 'top', 'FontSize',
         font_size);
74
75  xlabel('time [s]', 'FontSize', font_size);
76  ylabel('velocity [mm/s]', 'FontSize', font_size);
```

```
77 legend('2000  m  (Q = 1014.8)', '960  m  (Q = 2456.1)', '490  m  (Q =
       4575.6)', '183  m  (Q = 17038.3)', '54  m  (Q = 152273.3)', 'Location
       ', 'southeast', 'FontSize', font_size);
```

Appendix D

MATLAB code Figure 2.4a

```
clear
close all
clc

% Set font size
font_size = 13;

% Load COMSOL simulation data from Excel
levitationHeight_file = 'Levitation height.xlsx';
levitationHeight_sheet = 'Blad1';
levitationHeight_data = readtable(levitationHeight_file, 'Sheet',
    levitationHeight_sheet, 'Range', 'B2:N5');
levitation_height = table2array(levitationHeight_data(:, [1, 4, 7, 10,
    13])) / 1000;  % Columns B, E, H, K, N, converted to mm
particle_size = [2000, 960, 490, 183, 54] / 1000;  % Given particle
    sizes, converted to mm

levitation_height_simulation = [0.21304, 0.21015, 0.20515, 0.1945,
    0.17298, 0.13045];  % Simulation data
particle_size_simulation = [2000, 990, 490, 240, 115, 52.5] / 1000;  %
    Simulation particle sizes, converted to mm

% Fit a curve to the simulation data using power-law fitting
fit_result = fit(particle_size_simulation', levitation_height_simulation
    ', 'power2');

% Smooth curve points
smooth_particle_size_simulation = linspace(min(particle_size_simulation)
    , max(particle_size_simulation), 10000);
smooth_levitation_height_simulation = feval(fit_result,
    smooth_particle_size_simulation);

% Plotting
figure;
hold on;
h_measurement = scatter(particle_size, mean(levitation_height, 1), 50, '
    b', 'filled');  % Scatter plot of mean measurement data
```

```
errorbar(particle_size, mean(levitation_height, 1), std(
    levitation_height, 0, 1), 'b', 'LineStyle', 'none');  % Error bars
    for measurement data
h_simulation = plot(smooth_particle_size_simulation,
    smooth_levitation_height_simulation, 'r--');  % Smooth line plot of
    simulation data
hold off;

xlim([min([particle_size, particle_size_simulation]) - 0.1, max([
    particle_size, particle_size_simulation]) + 0.1])
ylim([min([levitation_height(:); levitation_height_simulation(:)]) -
    0.05, max([levitation_height(:); levitation_height_simulation(:)]) +
    0.05])
xlabel('Graphite Particle Size [mm]', 'FontSize', font_size);
ylabel('Levitation Height [mm]', 'FontSize', font_size);
set(gca, 'FontSize', font_size); % Set font size for tick labels and
    axis labels
grid on;

% Set the legend with font size
lgd = legend([h_measurement, h_simulation], {'Measurement', 'Simulation'
    }, 'Location', 'northwest', 'FontSize', font_size);
```

Appendix E

MATLAB code Figure 2.4b

```
clear
close all
clc

% Define font size
font_size = 13;

% Input data
frequency = [33.28, 34, 34, 34.81, 34.63];
particle_size = [2000, 960, 490, 183, 54] / 1000;

% Input simulation data
simulation_frequency = [31.6275, 31.6321, 31.7059, 31.8879, 32.2828,
    33.3507];
simulation_particle_size = [2000, 990, 490, 240, 115, 52.5] / 1000;

% Create a cell array of strings for particle sizes
particle_labels = cellstr(num2str(particle_size', '%.2f mm'));

% Set colors for the measurement and simulation data
measurement_color = [0, 0, 1]; % Blue color
simulation_color = [1, 0, 0]; % Red color

% Fit a curve to the simulation data using power-law fitting
fit_result = fit(simulation_particle_size', simulation_frequency', '
    power2');

% Smooth curve points
smooth_simulation_particle_size = linspace(min(simulation_particle_size)
    , max(simulation_particle_size), 10000);
smooth_simulation_frequency = feval(fit_result,
    smooth_simulation_particle_size);

% Plotting
figure;
hold on;
scatter(particle_size, frequency, 50, measurement_color, 'filled');
```

```
% Scatter plot of simulation data is replaced with a line plot for smoothness
plot(smooth_simulation_particle_size, smooth_simulation_frequency, 'r--');
hold off;
xlim([min([particle_size, simulation_particle_size]) - 0.1, max([particle_size, simulation_particle_size]) + 0.1])
ylim([30, 37])
xlabel('Graphite Particle Size [mm]', 'FontSize', font_size);
ylabel('Frequency [Hz]', 'FontSize', font_size);
set(gca, 'FontSize', font_size); % Set font size for tick labels and axis labels
grid on;

% Set the legend using custom colors and font size
lgd = legend('Measurement', 'Simulation', 'Location', 'best', 'FontSize', font_size);
```

Appendix F

MATLAB code Figure 2.4c

```
clear
close all
clc

% Set font size
font_size = 13;

% Set axis limits
xmin = 3e-2;
xmax = 3;
ymin = 2.5e2;
ymax = 0.7e6;

% Load COMSOL simulation data from Excel
comsol_file = 'comsol_data.xlsx';
comsol_sheet = 1;
comsol_range = 'F:G';
comsol_data = readtable(comsol_file, 'Sheet', comsol_sheet, 'Range',
    comsol_range, 'VariableNamingRule', 'preserve');
comsol_particle_size = comsol_data{:, 1};
comsol_q_factor = comsol_data{:, 2};

% Load measurement data from Excel
measurement_file = 'measurement_data.xlsx';
measurement_sheet = 1;
measurement_range = 'A:Z';
measurement_data = readtable(measurement_file, 'Sheet',
    measurement_sheet, 'Range', measurement_range, 'VariableNamingRule',
    'preserve');
measurement_particle_size = measurement_data{:, 1};
measurement_values = measurement_data{:, 2:end};

% Calculate the mean and standard deviation for each particle size,
    ignoring NaN cells
mean_measurement_values = nanmean(measurement_values, 2);
measurement_errors = nanstd(measurement_values, 0, 2);

```

```
% Scale the measurement errors
scaling_factor = 10; % Increase the error bars size
measurement_errors = scaling_factor * measurement_errors;

% Create a new figure with logarithmic scales
figure;
hold on;

% Set the marker color for the measurement dots to blue
marker_color = 'b';

% Plot the COMSOL simulation data in red (appearing second in the legend)
h_sim = plot(comsol_particle_size, comsol_q_factor, 'r--', 'LineWidth', 1, 'DisplayName', 'Simulation');

% Plot the measurement data with error bars and blue marker color (appearing first in the legend)
h_meas = errorbar(measurement_particle_size, mean_measurement_values, measurement_errors, 'o', 'LineWidth', 1, 'MarkerFaceColor', marker_color, 'MarkerEdgeColor', marker_color, 'Color', marker_color, 'DisplayName', 'Measurement');

% Set axis labels and title
xlabel('Graphite Particle Size [mm]');
ylabel('Q Factor');

% Adjust the axis limits
xlim([xmin, xmax]);
ylim([ymin, ymax]);

% Set logarithmic scale for both x-axis and y-axis
set(gca, 'XScale', 'log');
set(gca, 'YScale', 'log');

% Add the legend with "Measurement" (blue) and "Simulation" (red dotted line) entries
lgd = legend([h_meas, h_sim], 'Location', 'best');
set(lgd, 'FontSize', font_size); % Set legend font size

% Set font size for labels and tick labels
set(gca, 'FontSize', font_size);

% Adjust the plot appearance
grid on;
```

Appendix G

Laser cutter parameters

In the table provided below, we present two distinct configurations for the LASEA laser cutter, showcasing its versatility in accomplishing different tasks. The settings are divided into two categories: Blue and Red, each denoting specific functions in the laser cutting process.

Blue Settings: Cutting Out 2x2mm Plate

The entries marked with the color parameter set to Blue represent the cutting parameters utilized for the precise task of cutting out a 2x2mm plate from a larger substrate.

Red Settings: Cutting Pattern into Plate

Conversely, the entries highlighted with the color parameter set to Red outline the cutting parameters used for a different purpose: engraving intricate patterns onto a plate. In this mode, the LASEA laser cutter functions as an engraving tool, meticulously etching the prescribed design onto the plate's surface.

Delays	
LaserOn Delay	260
LaserOff Delay	260
Jump Delay	300
Mark Delay	300
Polygon Delay	0
Layer Delay	0
Design	
Color	Blue
Global	
Speed	50
Jump Speed	50
Burst Rate	25000
Burst Time	10
Repetitions	400
Sky Writing	False
Laser	
Pulse Rate	75018
Power	25

Delays	
LaserOn Delay	260
LaserOff Delay	260
Jump Delay	300
Mark Delay	300
Polygon Delay	0
Layer Delay	0
Design	
Color	Red
Global	
Speed	50
Jump Speed	50
Burst Rate	25000
Burst Time	10
Repetitions	100
Sky Writing	False
Laser	
Pulse Rate	75018
Power	7

Table G.1: Cutting parameters for the LASEA laser cutter.

Appendix H

Literature review

High-Q diamagnetically levitating resonators

Literature review

Eli Weisz

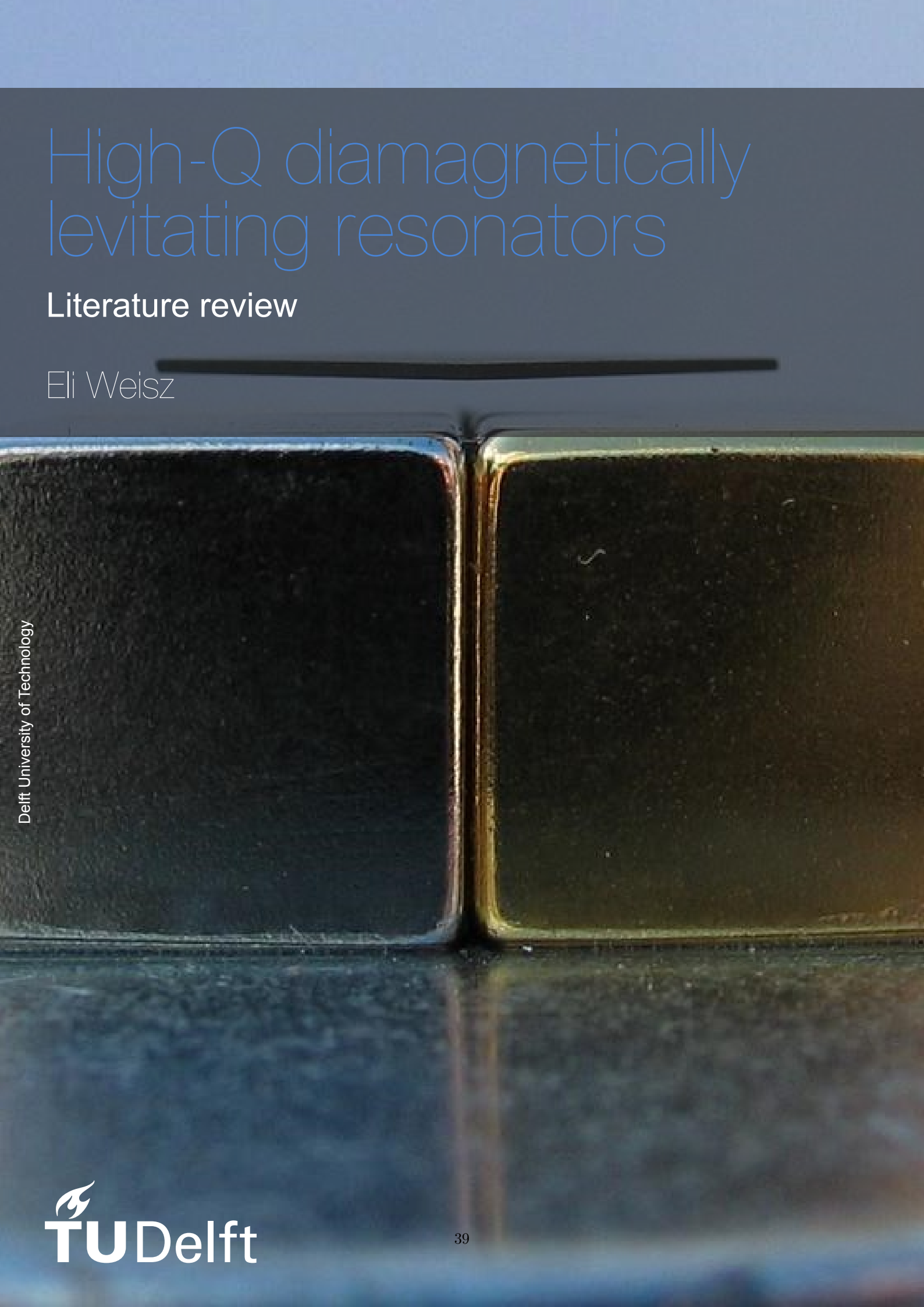

Delft University of Technology

TU Delft

High-Q diamagnetically levitating resonators

Literature review

by

Eli Weisz

Student Number 4459482

Supervizers Xianfeng Chen
Farbod Alijani

Delft University of Technology
Delft, Netherlands

TU Delft

Contents

List of Figures

1

Introduction

From the beginning of mankind, levitation has been an exciting phenomenon. Birds seemingly hovering high up in the sky awaiting their chance to dive down on their unsuspecting prey. Many stories have been told and written down about people levitating, for instance in the Bible. In the past centuries, a lot of research has been done on magnetism and levitation. By now it's well understood and implemented in many applications because there is no mechanical contact. This gives the opportunity for isolation from its environment and avoiding for instance mechanical friction in the case of a maglev train levitating above a track [1]. Or a chemical reaction conducted contact-free without containers or handling that might affect the outcome [2].
There are many ways to achieve levitation, for instance, by the use of magnets, superconductors, electric fields, laser beams, and sound waves. Magnets though can have a very distinctive feature, only with the combined use of permanent magnets and a diamagnetic material can stable levitation at zero power be achieved. This opens up great possibilities for realizing resonant energy harvesters and sensors. But in order to optimize these applications, a high quality factor is necessary. This literature review will focus on what influences the quality factor in a diamagnetically levitating resonator and how it can be improved.

2

Levitation

Levitation of micro- and nano-objects and their control of them while levitating has been of great interest to scientists for a while. A number of physical phenomena can be used for stable levitation, such as sound waves or beams of laser light, using a combination of magnets and superconductors, having charged particles in alternating electric fields, and using a diamagnetic material on an electromagnet or permanent magnet [3]. Levitation is used for many applications, for instance, containerless processing and investigation of materials, frictionless bearings, and high-speed ground transportation, for spectroscopy of single atoms and micro- and nano-particles, and for resonant sensors and energy harvesters [3, 4].

2.1. Magnetic levitation

Magnetic levitation comes in a few forms, the ”regular” one with permanent magnets or electromagnets or a combination of both. There is also superconductive levitation and diamagnetic levitation.

2.1.1. Magnets

Levitation with solely classic magnets without any stabilization technique can never be stable levitation, as shown by Earnshaw's theorem [5]. Such a technique could for instance be rotation, hence the gyroscopic effect, as shown in Figure 2.1 on the left. It can also be achieved by active controls, measuring the speed and position of the levitated object, and using a feedback loop to continuously adjust one or more electromagnets to keep the levitated object stably levitated. This is for instance used on maglev trains. Another stabilization technique would be to use mechanical support, for instance, a rod. This makes it possible to get free pseudo-levitation, an example is shown in Figure 2.1 on the right.
The upsides of using permanent and/or electromagnets are that they can lift large and heavy objects such as trains and cars. There is a possibility for free pseudo-levitation and because of this, the system can vibrate. The vibrations can be used for energy harvesters for instance [6, 7]. The downsides however are that because of this pseudo-levitation you will always lose energy in the stabilization technique.

Figure 2.1: On the left magnetic levitation stabilized using rotation is shown [8]. On the right Pseudo-levitation of two permanent magnets on a guide rod is shown [9].

2.1.2. Superconductive

Superconductive levitation is more accurately known as quantum levitation or quantum locking [10]. This is a quantum state in which a superconductor can levitate over a magnet or vice versa. The term quantum locking seems a bit more accurate since the levitated superconductor is really locked in space. The magnet can for instance be freely rotated without the superconductor moving with respect to the magnetic field lines of the magnet. This is caused by the Meissner effect, which occurs when a superconductor is cooled below its critical temperature and becomes superconductive. The magnetic field lines, instead of running through the superconductor, are ejected by the superconductor as shown in Figure 2.2 on the left. Since nothing in this universe is perfect, not all the lines are ejected by the superconductor. They will still move through the superconductor, but they cluster together. This phenomenon is called flux pinning and is shown in Figure 2.2 on the right. Superconductive levitation is great for stably levitating objects. When a magnet is suspended above a superconductor it's stably levitated, but it can still vibrate. Again these vibrations can be used for energy harvesting or measurements.

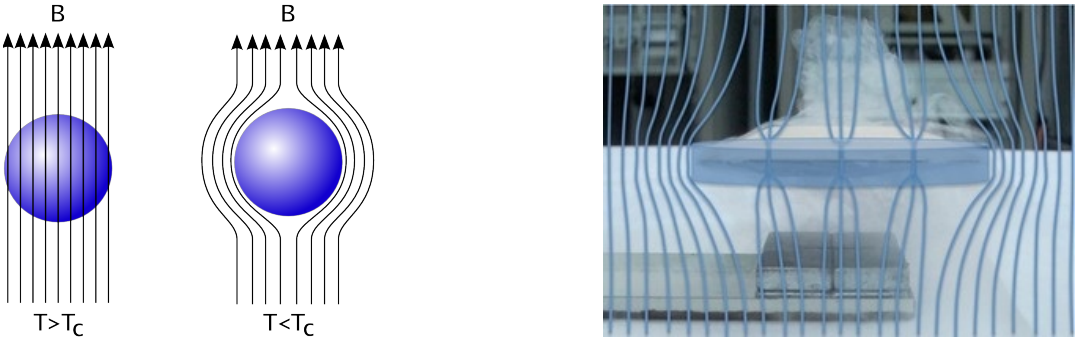

Figure 2.2: On the left expulsion of magnetic field lines is shown [11]. On the right flux pinning and the magnetic field lines that are associated with it are shown [12].

2.1.3. Diamagnetic

Diamagnetism is a quantum mechanical effect that occurs in all materials. This causes the material to be repelled by a magnetic field. Even though all materials have a diamagnetic effect, not all materials are diamagnetic. If the magnetic effects overcome the diamagnetic effect, that specific material would be magnetic. A magnetic field, independent of its direction, creates an induced magnetic field in the diamagnetic material, causing a repulsive force. As mentioned before, all materials are diamagnetic, but if a material has a greater magnetic effect than diamagnetic effect, the material is said to be magnetic. The great difference between diamagnetic levitation and magnetic levitation is that with diamagnetic levitation stable levitation is possible without the use of any stabilization technique. This makes stable and free levitation possible [13].

2.2. Electric levitation

Electric levitation is used to levitate charged particles in an electric field.

2.2.1. Electrostatic

Electrostatic levitation is a form of levitation in which a charged particle is levitated in an electric field. Just like with subsection 2.1.1 electrostatic levitation is also never stable without any stabilization technique [5]. A much-used stabilization technique for electrostatic levitation is covered in subsection 2.2.2.

2.2.2. Quadrupole ion trap

The quadrupole ion trap also called a Paul trap, is a form of electrostatic levitation capable of levitating a charged particle stably. This is achieved by placing a charged particle between four plates with a changing potential in time, this is shown in Figure 2.3.

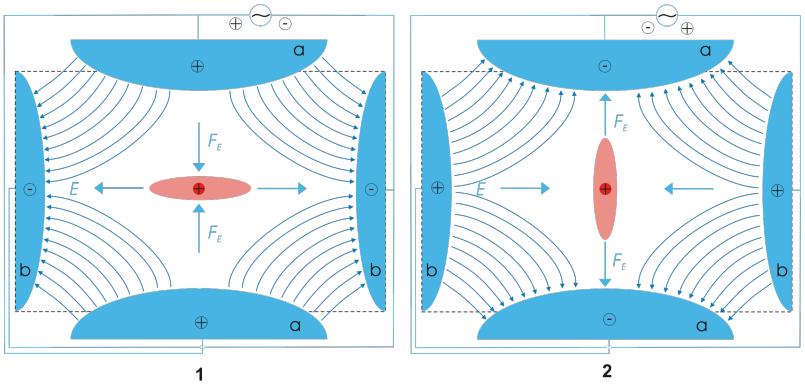

Figure 2.3: Changing potential of a quadrupole ion trap [14].

The positively charged particles are shown in red. The blue area's are the plates with a positive or negative charge and the blue arrows indicate the direction of the electric field. The positively charged particles in the center of the ion trap are rotating within the electric field. At the center of the positively charged particle cloud the particles are stably levitated.

2.3. Optical levitation

Optical levitation can be achieved by optical tweezers (originally called a single-beam gradient force trap). This is a way of holding and moving small (nano- to micron-sized [15]) dielectric particles using a focused laser beam. When this is done in air or vacuum and a particle can be held without any form of support besides the laser beam, it can be called optical levitation.

The laser creates an attractive force towards the center of the laser beam (the laser intensity has a gradient being the highest in the center) due to the conservation of momentum. This force (usually in the order of piconewtons) depends on the relative refractive index between the particle and surrounding medium [16]. When looking at Figure 2.4 at the unfocused laser beam, it can be seen that when the particle leaves the center of the beam there is a net force (F_{net}) towards the center because of the photons changing direction due to the refraction of the light by the particle. Notice that when there is no force counteracting this F_{net} the particle will keep moving away from the laser beam origin. This can be solved by using a focused laser beam as can be seen in Figure 2.4. Using a focused laser beam the particle can be kept around the beam waist (the narrowest point of the focused beam).

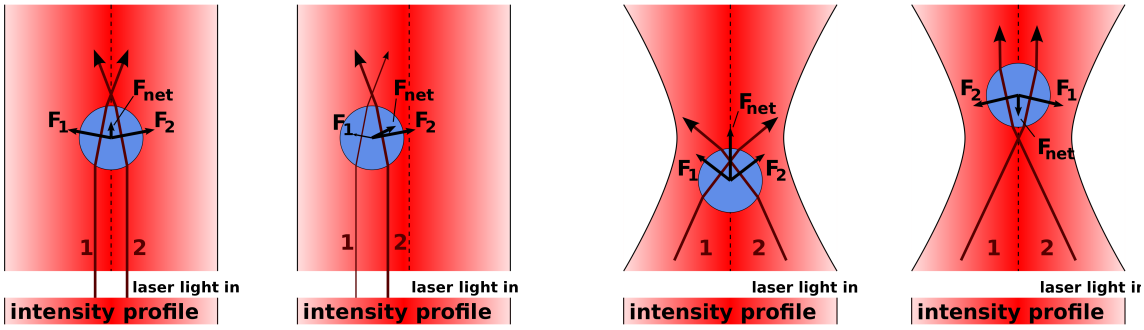

Figure 2.4: On the left an unfocused laser beam trapping a particle can be seen [17]. On the right a focused laser beam trapping a particle can be seen [18].

For optical tweezers the expression of the quality factor is shown in Equation 4.3, with trapping force F, laser power P, light velocity c, and refractive index of the medium n_1 [19].

$$Q = \frac{Fc}{Pn_1} \tag{2.1}$$

2.4. Acoustic levitation

Acoustic levitation is a way of levitating objects using high-intensity sound waves. The high intensity is necessary to overcome the gravitational acting on the levitating objects. It is also the only levitation technique that depends solely on the material density and size of the object (depending on the wavelength) and not the electrical charge, magnetic susceptibility, or refractive index. Another advantage is that it can suspend both liquids and solids. There are several possible setups for acoustic levitators as can be seen in Figure 2.5.

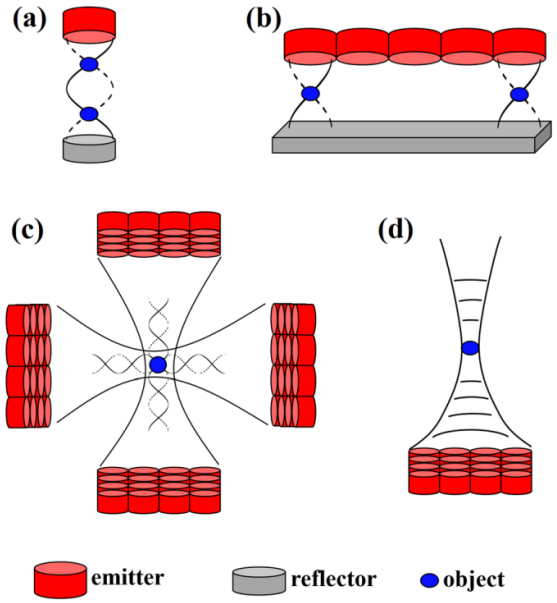

Figure 2.5: Schematic of different types of acoustic levitators. (a) Single-axis acoustic levitator. (b) Two-dimensional manipulation of multiple drops using an array of Langevin-type transducers and an opposing reflector. (c) Three-dimensional manipulation of levitated particles using four orthogonal arrays of ultrasonic emitters. (d) Single-beam trapping. [20].

The single beam and two-dimensional levitators can only be used to trap an object and are relatively unstable in the direction perpendicular to the sound wave. The three-dimensional levitator is however stable in all directions and can even be used for controlled manipulation of the object by changing the frequencies of the sound waves in certain directions. The stable point for objects to levitate is at the point of minimal force, which is where the sound waves cancel each other out. This is somewhat similar to the stable point in a focused laser beam as discussed in section 2.3 and shown in Figure 2.4.

2.5. Comparison

Table 2.1 shows a comparison of the pros and cons of the different levitation techniques discussed in chapter 2.

	Magnets	Superconductive	Diamagnetic	Electrostatic	Quadrupole ion trap	Optical	Acoustic
Passive levitation	✓	x	✓	x	x	x	x
Stable levitation without any stabilization technique	x	✓	✓	x	✓	x	x
Vacuum compatibility	✓	✓	✓	✓	✓	✓	x
Ability to levitate macro scale	✓	✓	✓	x	x	x	x
Ability to levitate any material	x	x	x	x	x	x	✓

Table 2.1: A comparison of the different levitation techniques.

3

Diamagnetism

3.1. Materials

Diamagnetic materials, unlike magnetic materials, are always repelled by a magnetic field. An applied magnetic field in a diamagnetic material creates an induced magnetic field in the opposite direction, causing a repellent force. This property in combination with an inhomogeneous magnetic field can be used for stable and free levitation [13].
The relation between the magnetization of a material $(\mathbf{M})$ and the magnetic field strength $(\mathbf{H})$ is defined as:

$$\mathbf{M} = \chi_v \mathbf{H}$$

From this, it can be seen that diamagnetic materials have a volume magnetic susceptibility (χ_v) less than or equal to 0 in order to get an opposing magnetic field compared to the magnetic field source. The strongest type of diamagnets is superconductors. Superconductors can be considered to be perfect diamagnets since $\chi_v = -1$ [21]. The downside of superconductors is the fact that they need to be kept very cold. For instance, $SmFeAsO1{-}\delta$, which is a high-temperature superconductor, has its critical temperature at $55K$ [22].
When looking at Table 3.1 it can be seen that there are more materials with diamagnetic properties (this table only shows a few other materials, there are many more). Actually, all materials have a diamagnetic effect, not all materials are diamagnetic. If the magnetic effects overcome the diamagnetic effect, that specific material would be considered magnetic and not diamagnetic.

Table 3.1: Notable diamagnetic materials [21].

Material	$\boldsymbol{\chi_v[\times 10^{-5}]}$
Superconductor	-10^5
Pyrolytic carbon	-40.9
Bismuth	-16.6
Neon	-6.74
Mercury	-2.9
Silver	-2.6
Carbon (diamond)	-2.1
Lead	-1.8
Carbon (graphite)	-1.6
Copper	-1.0
Water	-0.91

One material that might not be the first that comes to mind when thinking about diamagnetism is water. In 1997 one of the most interesting experiments concerning diamagnetic levitation was done. The researchers managed to levitate small objects such as live frogs (Figure 3.1), grasshoppers, waterdrops (Figure 3.1), flowers and hazelnuts [23]. For this experiment, they used a 20 Tesla Bitter solenoid

at around $16T$ at the Nijmegen High Field Magnet Laboratory. The electromagnet consumed $4MW$ during the experiment, which is way too much for daily use. The researchers won the Ig Nobel Prize in 2000 for this study.

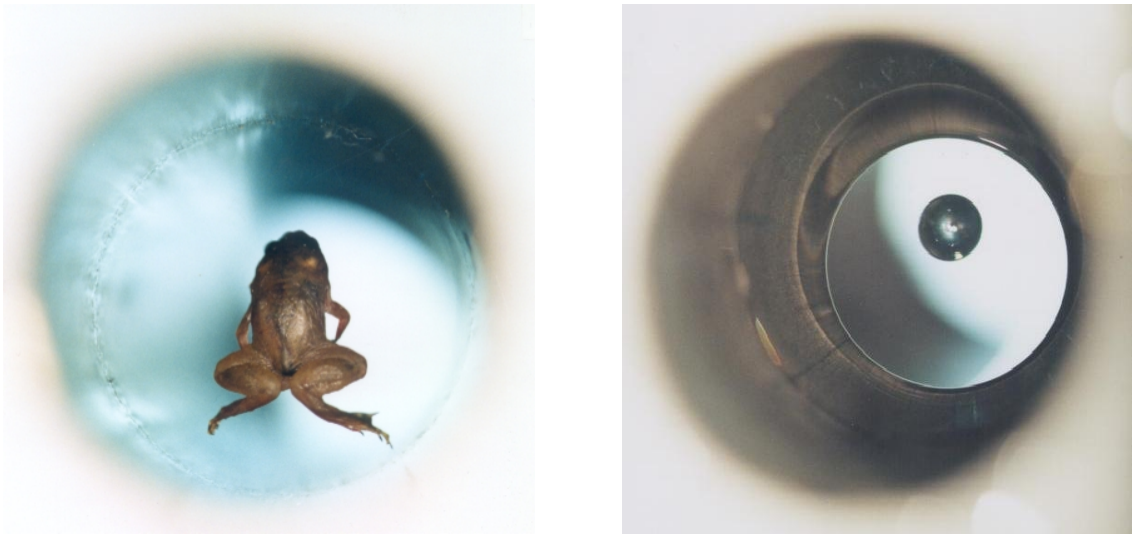

Figure 3.1: A frog and a waterdrop levitate inside a Ø32mm vertical bore of a Bitter solenoid in a magnetic field of about $16T$ [23, 24].

But besides water, as can be seen in Table 3.1, there are more materials that have a higher magnetic susceptibility than water, with the advantage that this property is there at room temperature. This makes levitation at zero power possible. In recent years levitation of liquid droplets [25, 26], cells [27], and solid particles [26] have been demonstrated using small permanent magnets.

The most interesting material to use nowadays, also shown in Table 3.1, is pyrolitic graphite. The properties of pyrolitic graphite are shown in Table 3.2

Table 3.2: Properties of pyrolitic graphite [4].

Property	Symbol	Value	Unit
Density	ρ	2070	kg/m^3
Susceptibility $\perp$	χ_z	-450	$\times 10^{-6}$
Susceptibility $\parallel$	$\chi_{x,y}$	-85	$\times 10^{-6}$
Conductivity $\perp$	σ_z	200	S/m
Conductivity $\parallel$	$\sigma_{x,y}$	200000	S/m

3.2. Applications

As mentioned in section 3.1 with a relatively strong diamagnetic material at room temperature and the use of strong permanent magnets, it is possible to achieve levitation at a small scale of the diamagnetic material at zero power. This gives a whole range of possible applications, such as accelerometers [28, 29], energy harvesters [30, 31, 32], viscosity and density sensors [33] and force sensors [34].

4

Quality factor

The quality factor also referred to as the Q factor, is a dimensionless parameter describing how underdamped an oscillatory system is. This means that $\zeta < 1$ with ζ being the damping ratio which is a non-dimensional characterization of the decay rate relative to the frequency of the oscillatory system. In other words, the higher the Q factor, the longer it takes for the oscillatory system to dampen out.

4.1. Damping

For diamagnetic resonators, the main sources of dissipation are air and eddy current damping [30, 32, 35]. When the resonator is operated in a vacuum, it's possible to eliminate air damping, so that the only remaining dissipative force is eddy current force, which can be minimized to obtain high Q resonators [4].

4.2. Air damping

The air damping for diamagnetic resonators is caused by the drag force through the air. This force can be relatively easily eliminated by operating diamagnetic resonators in a vacuum. It can be seen from earlier performed experiments that the influence of air damping on the Q factor is neglectable from about $10^{-3} mbar$, as can be seen in Figure 4.1.

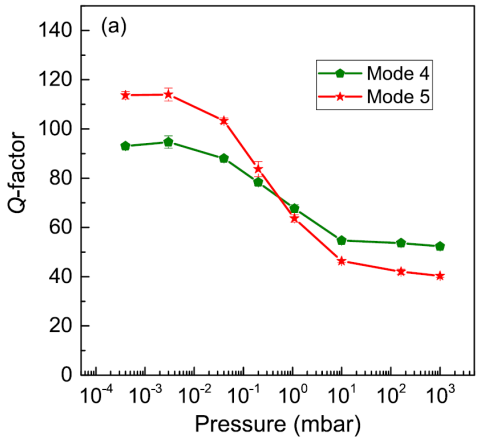

Figure 4.1: Pressure-dependent Q factor of a $8.03 \times 8.24 \times 0.28 mm^3$ levitating plate [4].

4.3. Eddy currents

Eddy currents are a physical phenomenon explained by Faraday's law of induction. Eddy currents are loops of an electric current induced by a changing magnetic field passing through an electric conductor. When for instance a disk is rotating through a stationary magnetic field, the magnetic flux in a given

area of the disk changes. When a given area of the disk is getting closer to the magnet the strength of the magnetic field increases $\left(\frac{d\mathbf{B}}{dt} > 0\right)$, then according to Faraday's law of induction, a current is created perpendicular to the direction of the magnetic field. When the disk is moving away from the magnet $\left(\frac{d\mathbf{B}}{dt} < 0\right)$, the same thing happens, but the current loop changes direction. An example of this is shown in Figure 4.2.

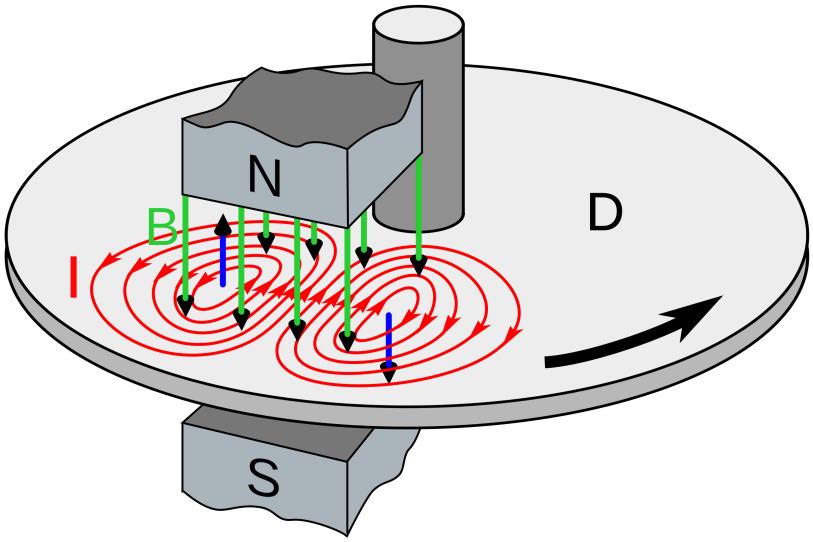

Figure 4.2: An example of eddy currents in an eddy current brake [36].

In Figure 4.2 it can be seen that the eddy currents (**I**) are induced by the disk (**D**) rotating through the magnetic field (**B**). The blue lines are magnetic field-created loops of electric current as stated by Ampere's circuital law. The **N** and **S** are the north and south poles of the stationary magnet respectively.

As shown above in section 4.3 eddy currents can be used as a brake [37, 38], this is due to the fact that eddy currents can dissipate a lot of power in the form of heat. This heat is created because the electric conductor has an electric resistance larger than zero.
The amount of power dissipated by the eddy currents per unit mass for a thin sheet is given by the following formula [39]:

$$P = \frac{\pi^2 B_p^2 d^2 f^2}{6\rho D} \tag{4.1}$$

In which P is the power lost per unit mass (W/kg), B_p is the peak magnetic field (T), d is the thickness of the sheet or diameter of the wire (m), f is the frequency (Hz), ρ is the resistivity of the material (Ωm), and D is the density of the material (kg/m^3).

Together with this power loss comes a drag force (F_2), which can be seen in Figure 4.3.

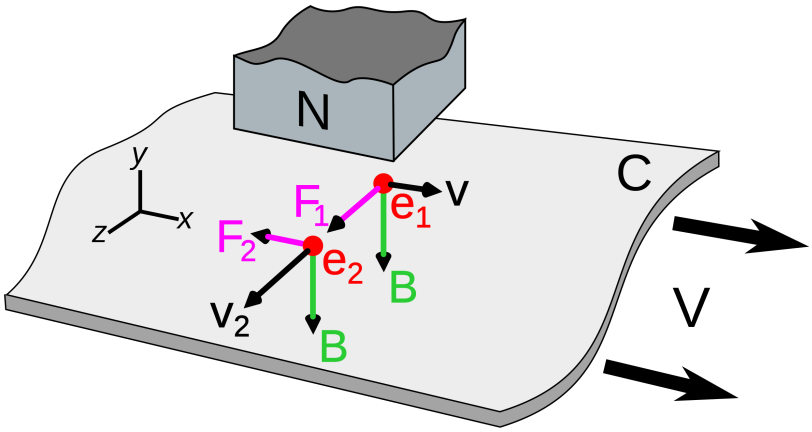

Figure 4.3: The movement of electrons causing a drag force [40].

When a sheet of a conductive material (C) is moving relative to a magnetic field, the electrons in this sheet travel in the same direction and with the same velocity (**v**) as the sheet. When the electron passes through the magnetic field a Lorentz force (F_1) is exerted on the electron (in this example e_1): $F_1 = -e\,(\mathbf{v}\times\mathbf{B})$, where e is the electron's charge. This Lorentz force causes the other electron (e_2) to be accelerated and therefore for it to get a sideways velocity ($\mathbf{v_2}$). Due to this velocity and the still present magnetic field, another Lorentz force ($F_2 = -e\,(\mathbf{v_2}\times\mathbf{B})$) is exerted on e_2 in the direction opposite from the velocity (**v**). In a sheet passing through a magnetic field, a Lorentz force is exerted on a large number of electrons. The sum of these Lorentz forces is the drag force experienced by the moving sheet.

5

State of the art

When, as mentioned in section 3.2, you want to use diamagnetic levitation for accelerometers, energy harvesters, and sensors, it's important to have the least amount of damping possible to achieve a high quality factor. When a pyrolytic graphite plate is levitated over magnets and made to vibrate, a magnetic flux change occurs in the plate, which induces eddy currents, which leads to drag forces and thus damping (as mentioned in section 4.3 shown in Figure 4.3).
It is important to minimize the number of eddy currents in the pyrolytic graphite plate.
One way of doing this is by reducing the pyrolytic graphite plate size, the smaller the size, the fewer eddy currents can exist, this can be seen on the right side in Figure 5.1. The downside of this is that the smaller the plate gets, the smaller the objects (for instance droplets) we can levitate on the plate become. In an attempt to preserve the macro-scale levitation but reduce the "plate size" pyrolytic graphite micro-particles (powder) were put in an electric insulating composite. If the particles don't touch the eddy currents can't flow freely and they will therefore occur less [41]. This results in an increase of the Q factor. An example of this can be seen on the left side of Figure 5.1.

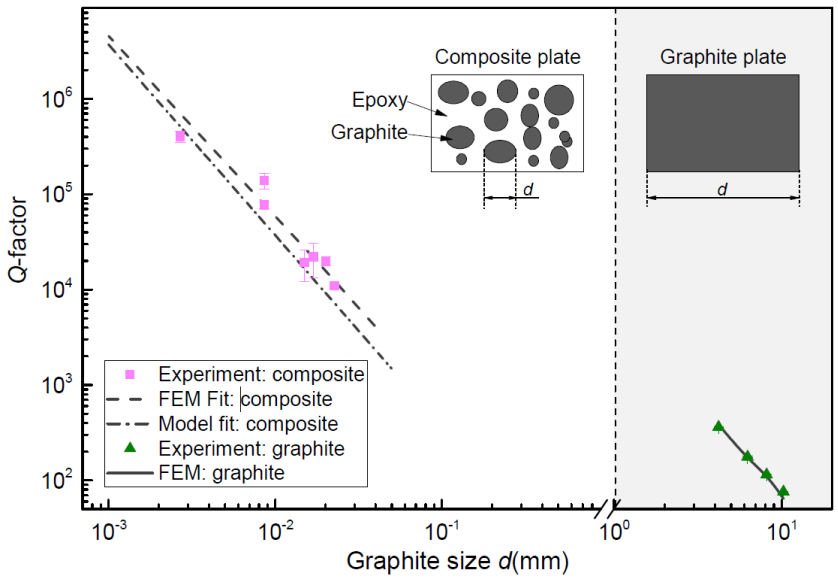

Figure 5.1: The influence of the pyrolytic graphite size on the Q factor [41].

In the experiments, shown in Figure 5.1, a Q factor as high as 0.5 million was reached when using a graphite powder with a particle size of $2.7{-}22.7\mu m$ was dispersed in Epotek 302-3M epoxy [41].

The setup in which these measurements were done can be seen in Figure 5.2.

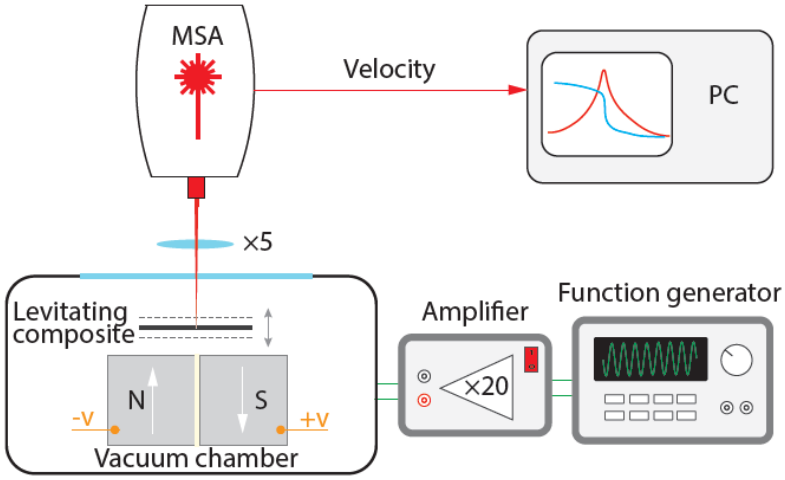

Figure 5.2: Schematic of the measurement setup [41].

The setup comprised of an MSA400 Polytec laser Doppler vibrometer (LDV) for the readout and the electrostatic excitation method. The actuation voltage is generated by the function generator and is amplified by a $20\times$ voltage amplifier that drives the levitating diamagnetic plate into resonance. The electrostatic force is generated via the magnets which are connected to electrodes beneath the levitating plate. The magnets are separated by Kapton tape for insulation. By focusing the MSA laser beam on the plate, the vibration signal is detected, and the acquired velocity is transferred to a PC for spectral analysis [41].

5.1. Modelling

Measuring the exact location and direction of eddy currents isn't possible. So to quantify the eddy current damping of the levitating resonator, a FEM model was developed to evaluate the eddy current damping force [4]. The multiphysics simulation software used in this case is COMSOL. Using this a visual model can be made to get a better understanding of how the eddy currents are distributed throughout the material. An example of this can be seen in Figure 5.3.

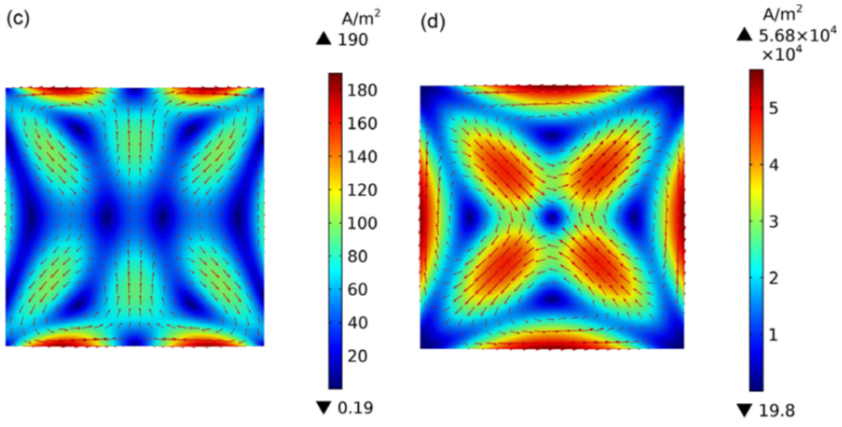

Figure 5.3: Visualization of eddy currents using COMSOL [4].

In this figure, the eddy current density simulations of two different rigid body modes of a diamagnetically levitating graphite plate can be seen.

The model can also be used to predict the Q factor as a function of plate length L (where the plate thickness t and magnet size D are also scaled ($D = 1.2L$ and $t = 0.03L$)). This is shown in Figure 5.4.

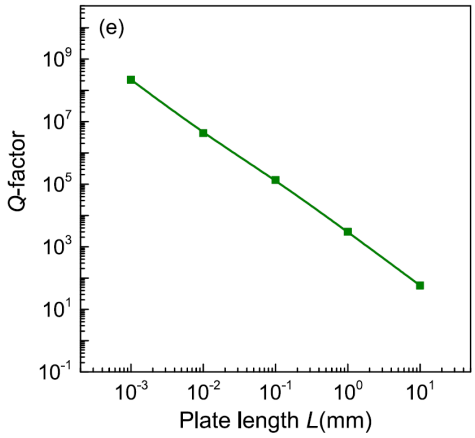

Figure 5.4: Simulation of the Q factor as a function of plate length L [4].

5.2. Problem

When comparing the Q factor from the simulation Figure 5.4 to the Q factor from the measurements done with the pyrolytic graphite powder plate Figure 5.1. It can be seen that for equal length ($d = L$), the Q factor from the measurements is much lower than the theory.
This is caused by the graphite micro-particles not fully separating from each other, this is shown in Figure 5.5.

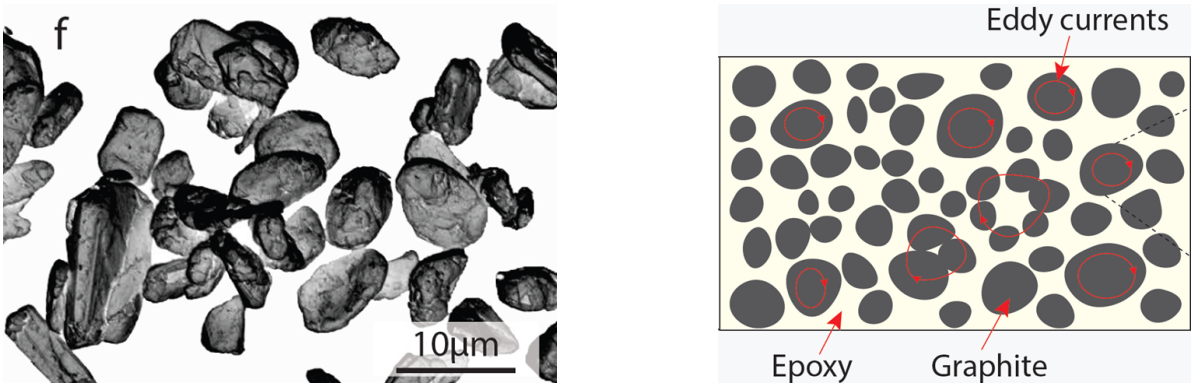

Figure 5.5: The left figure shows an electron microscopy image of the size and morphology of the graphite particles. The right figure shows a schematic of the eddy currents generated inside the graphite micro-particles that are distributed in the composite [41].

When the micro-particles are touching each other they act in the same way as one larger micro-particle, creating a larger plate length and more eddy currents, which results in a lower Q factor.
The clustering of the micro-particles is a problem that has to be resolved.

Therefore the main research question resulting from this literature review is:

How can the distribution of the graphite micro-particles be controlled and thus ensure that no micro-particles are making contact to reduce the eddy currents and therefore increase the quality factor without losing the ability to levitate macro-scale objects?

Also a sub-objective results from the literature review:

the existing FEM model to quantify the eddy current damping should be verified.

6 Research

In the latest research on diamagnetically levitating graphite resonators, quality factors as high as 0.5 million (Figure 5.1) were obtained by insulating graphite particles using an epoxy matrix, as shown in chapter 5. The future goal is to increase the quality factor even further to a million or higher. The biggest factor in increasing the Q factor is decreasing the eddy currents in the pyrolytic graphite plate. Several ways to realize this are shown in Figure 6.1.

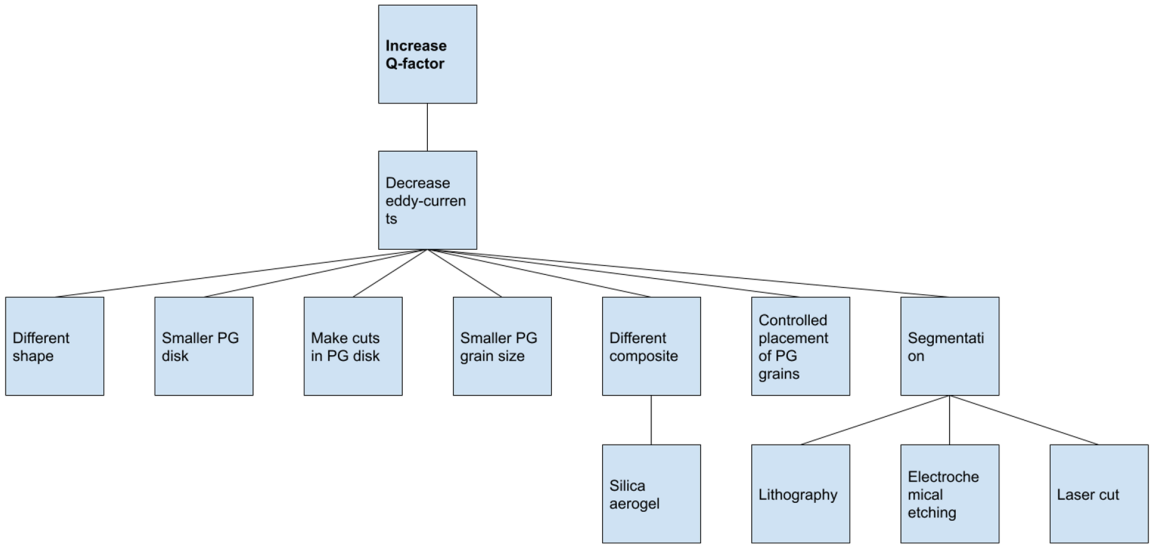

Figure 6.1: Several ways to decrease eddy currents and increase the Q factor.

Trying different outer shapes for the graphite plate would be an option, this may slightly interrupt the path of the eddy currents, but for the most part, they would still be able to move freely through the material.
Decreasing the size of the graphite plate would work, the smaller the material, the fewer eddy currents can exist as shown in chapter 5. The downside of this is losing the ability to levitate macro-scaled objects, whilst this is an important property to maintain.
Making cuts in the graphite plate can reduce eddy currents, but making random cuts may not give a satisfying outcome. For instance, making cuts in places where there are few eddy currents decreases the ability to levitate macro-scaled objects, but doesn't reduce the eddy currents much. But this could be an interesting method once a verified FEM model has been made and cuts can be made in places where eddy currents are predicted to be dominant.
Using a finer pyrolytic graphite powder than the one used in previous experiments will increase the Q factor (Figure 5.1). But making a finer powder than the used $2.7{-}22.7\mu m$ size is difficult. This also

wouldn't solve the clustering problem mentioned in section 5.2.
Using a different composite than Epotek 302-3M epoxy to disperse the graphite powder would be an option. If the composite has a lower density than the Epotek 302-3M epoxy, for instance, silica aerogel. In this case, less powder is needed to achieve levitation, but this still doesn't solve the clustering problem, though there would be less clustering because there are fewer particles in an equal volume, assuming an equal particle distribution.
Trying to position the graphite powder particles in a controlled way ensuring there is no clustering would be perfect, though there doesn't seem to be a way to achieve this with a powder dispersion in a composite.
When using segmentation of a solid piece of pyrolytic graphite instead of a powder dispersion, the placement of the segments can be accurately controlled ensuring no contact between the segments. If the segments can be made small enough, it is possible to achieve very high Q factors.
Three ways of creating these segments were investigated, the first one being lithography. There are two main types of lithography, photolithography, and electron-beam lithography. Photolithography is a patterning process in which a photosensitive polymer is selectively exposed to light through a mask, leaving a latent image in the polymer that can then be selectively dissolved to provide patterned access to an underlying substrate [42]. Current state-of-the-art photolithography tools use deep ultraviolet light with wavelengths of $248 - 193nm$, allowing feature sizes below $100nm$ to be printed with good yield [43]. The downside is that it's very expensive and difficult to use. Also, pyrolytic graphite isn't a material normally used with photolithography.
Electron-beam lithography has a lot in common with photolithography, but instead of sending light through a mask electron-beam lithography uses a focused beam of electrons to draw custom shapes on a surface. Features as small as $5nm$ and below have been fabricated using e-beam lithography [44]. This method is cheaper to use than photolithography, but also in this case pyrolytic graphite isn't a material normally used in this process.
Atomic force microscopy (AFM)-based electrochemical etching of pyrolytic graphite has been studied for single atomic layer lithography [45]. But it doesn't seem to be used for etching bigger structures.
Another way of cutting into a material is using a laser cutter. The feature size of laser cutting is larger than with the use of lithography, but it's much cheaper and easy to use. Another great advantage is that the Delft University of Technology already has one, so no investments or outsourcing has to be done. This machine has a cutting width of about $30\mu m$, which for the purpose of this research is sufficient.

6.1. Laser cutting

Laser cutting is a process in which a focused bursting laser beam vaporizes materials, resulting in a cut edge. When used for cutting pulsed lasers which provide a high-power burst of energy for a short period are very effective, particularly for piercing, or when very small holes or very low cutting speeds are required since if a constant laser beam is used, the heat could reach the melting point of the material.

Now, for making segments in a pyrolytic graphite plate, using the laser cutter the required steps are shown in Figure 6.2.

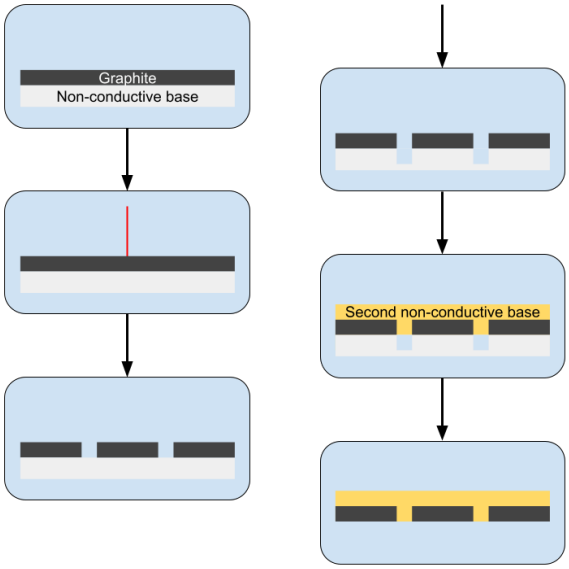

Figure 6.2: A side view of the steps required for segmenting a graphite plate using a laser cutter.

The first step is to apply a non-conductive base layer to the graphite plate, this can for instance be epoxy.
Secondly, the laser is programmed with the right parameters, such as laser power, cutting speed, and the number of repetitions. Also, the desired pattern is set and the laser is focused. Then the cutting begins.
Once finished the graphite is pierced, but the non-conductive base layer is also cut and weakened.
A new non-conductive base layer (doesn't have to be the same material) has to be applied.
The first non-conductive base layer can then be removed, giving a solid segmented pyrolytic graphite plate

6.2. First results

A few experiments have already been done. The first results of the laser cutting are shown in Figure 6.3.

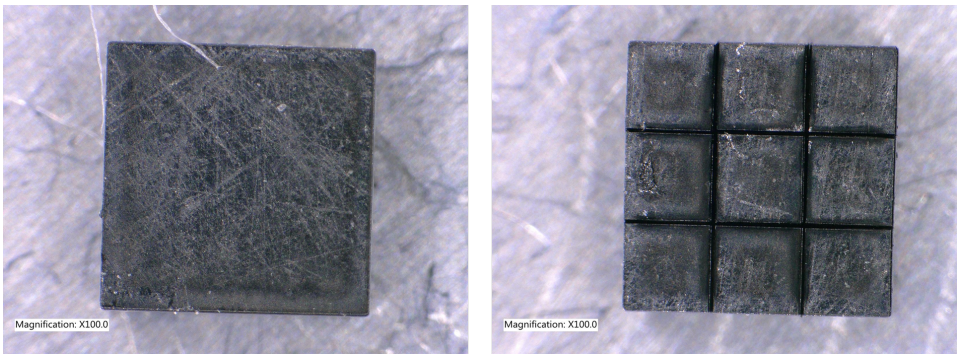

Figure 6.3: On the left side a graphite plate cut to $2 \times 2mm$ can be seen. On the right, there's a graphite plate of the same size, but with a 3×3 matrix cut into it.

Some first measurements were performed with these two plates, they were performed with the same measurement setup as mentioned in chapter 5 and shown in Figure 5.2.
The measurements were performed as followed: The excitation voltage is generated by the Polytec junction box, in case of resonance frequency measurements, or a function generator when a ring-down response is of interest. The electrostatic force is applied via the magnets which are directly connected

with two electrodes beneath the levitating plate. To isolate the magnets from one another Kapton tape is used. Since the electrostatic force is proportional to the square of the voltage, a DC offset voltage is added to make sure the electrostatic force has a component of the same frequency as the output voltage. Finally, to read out the motion, a Polytec LDV is used. The LDV measurements are conducted in a vacuum chamber at a pressure of about $10^{-5}mbar$ at room temperature [41].

After performing a ring-down fit the Q factor of both plates can be calculated, the results are shown in Figure 6.4.

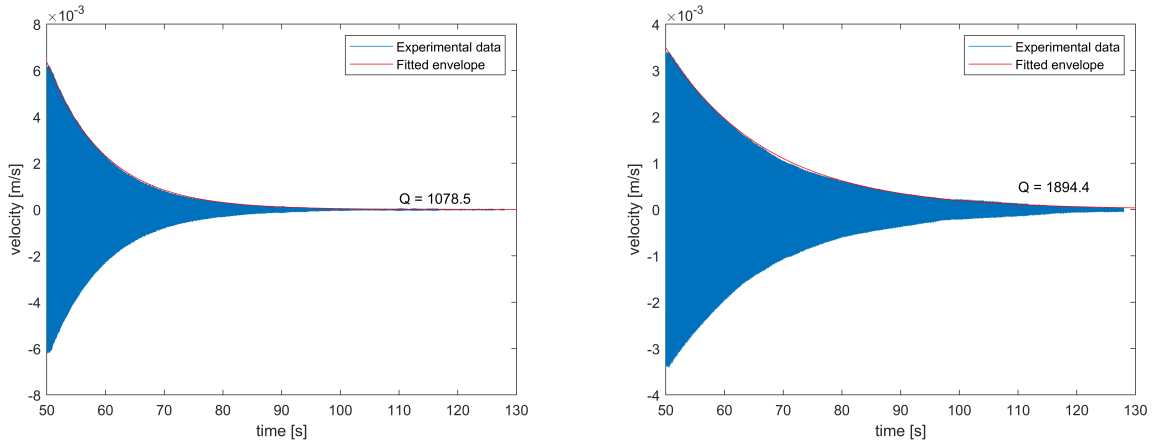

Figure 6.4: On the left, the result of the ring-down fit of the plate without cuts is shown. On the right, the result of the ring-down fit of the plate with cuts is shown.

It can be seen that the Q factor increases when the pyrolytic graphite plate is cut into segments, though it must be mentioned that the increase isn't as high as expected. Considering that a segment is roughly $0.6mm$ for the 3×3 matrix plate, comparing this to the theoretical model, the Q factor should have been around $6000 - 7000$.
After putting the 3×3 matrix plate under the microscope, it could be seen that the cuts didn't go completely through the graphite, this is shown in Figure 6.5. This most likely allowed eddy currents to still pass from one segment to the other, causing more eddy currents and thus a lower Q factor. In future experiments, this will have to be resolved by for instance using different laser parameters or a different non-conductive base layer.

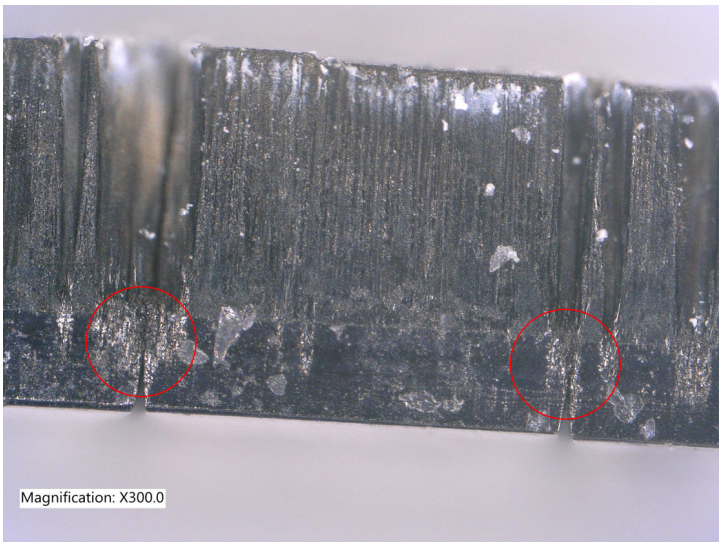

Figure 6.5: A side view of the 3×3 matrix plate under the microscope at a $3000\times$ magnification.

7

Timetable

In the upcoming months, the research question and sub-objective(s) have to be accomplished. A timetable is made to make sure the objectives are achievable within the available time frame.

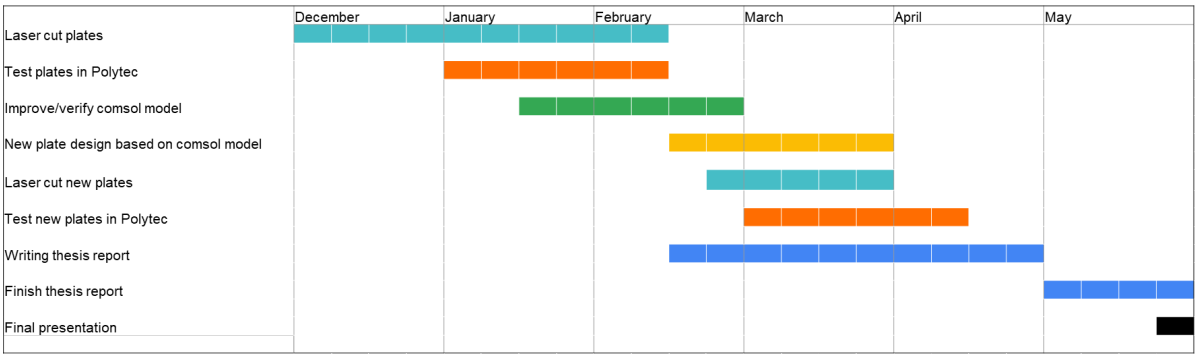

In December, January, and February pyrolytic graphite plates have to be cut and viewed under the microscope if the cuts are completely through.
During January and February measurements have to be done on the plates that were correctly cut. Using these measurements the FEM model (in COMSOL) can be verified and adapted when necessary. Halfway into February new plates based on the improved and verified COMSOL model should be designed and cut by the end of March.
From March till mid-April measurements have to be performed on these new plates, most likely several iterations are necessary here.
In the meantime from mid-February till the end of May, the thesis report has to be written and finished.

References

[1] Hyung-Woo Lee, Ki-Chan Kim, and Ju Lee. “Review of maglev train technologies”. In: *IEEE Transactions on Magnetics* 42.7 (2006), pp. 1917–1925. DOI: 10.1109/TMAG.2006.875842.

[2] Stephen Brotton and Ralf Kaiser. “Controlled Chemistry via Contactless Manipulation and Merging of Droplets in an Acoustic Levitator”. In: *Analytical Chemistry* 92 (June 2020). DOI: 10.1021/acs.analchem.0c00929.

[3] E. H. Brandt. “Levitation in Physics”. In: *Science* 243.4889 (1989), pp. 349–355. DOI: 10.1126/science.243.4889.349. eprint: https://www.science.org/doi/pdf/10.1126/science.243.4889.349. URL: https://www.science.org/doi/abs/10.1126/science.243.4889.349.

[4] Xianfeng Chen et al. “Rigid body dynamics of diamagnetically levitating graphite resonators”. In: *Applied Physics Letters* 116 (24 June 2020). ISSN: 00036951. DOI: 10.1063/5.0009604.

[5] S. Earnshaw. “On the Nature of the Molecular Forces which Regulate the Constitution of the Luminiferous Ether”. In: *Transactions of the Cambridge Philosophical Society* 7 (Jan. 1848), p. 97.

[6] Krzysztof Kecik and Andrzej Mitura. “Theoretical and Experimental Investigations of a Pseudo-Magnetic Levitation System for Energy Harvesting”. In: *Sensors* 20.6 (2020). ISSN: 1424-8220. DOI: 10.3390/s20061623. URL: https://www.mdpi.com/1424-8220/20/6/1623.

[7] Krzysztof Kecik et al. “Foldover effect and energy output from a nonlinear pseudo-maglev harvester”. In: *AIP Conference Proceedings* 1922.1 (2018), p. 100009. DOI: 10.1063/1.5019094. eprint: https://aip.scitation.org/doi/pdf/10.1063/1.5019094. URL: https://aip.scitation.org/doi/abs/10.1063/1.5019094.

[8] Roberto Arias. *Science show magnetic levitation*. [Online; accessed 20-July-2022]. 2010. URL: https://en.wikipedia.org/wiki/File:Science_show_magnetic_levitation.jpg.

[9] Antonín Ryska. *Pseudo-levitation of two permanent magnets on a guide rod*. [Online; accessed 14-September-2022]. 2017. URL: https://upload.wikimedia.org/wikipedia/commons/c/c0/Pseudo-levitation_of_two_permanent_magnets_on_a_guide_rod.jpg.

[10] Taha H Ababou. “Evolution of transportation systems with quantum levitation”. In: ().

[11] Piotr Jaworski. *Expulsion*. [Online; accessed 21-July-2022]. 2005. URL: https://commons.wikimedia.org/wiki/File:EXPULSION.png.

[12] *Flux Pinning Field Diagram*. [Online; accessed 26-July-2022]. 2012. URL: https://en.wikipedia.org/wiki/File:Flux_Pinning_Field_Diagram.jpg.

[13] Gerald Küstler. *Électrotechnique et électroénergétique DIAMAGNETIC LEVITATION-HISTORICAL MILESTONES*. 2007, pp. 265–282.

[14] Arian Kriesch Akriesch. *Paul-Trap*. [Online; accessed 15-August-2022]. 2006. URL: https://en.wikipedia.org/wiki/File:Paul-Trap.svg.

[15] Nan Li et al. “Review of optical tweezers in vacuum”. In: *Frontiers of Information Technology Electronic Engineering* 20 (May 2019), pp. 655–673. DOI: 10.1631/FITEE.1900095.

[16] A. Ashkin et al. “Observation of a single-beam gradient force optical trap for dielectric particles”. In: *Opt. Lett.* 11.5 (May 1986), pp. 288–290. DOI: 10.1364/OL.11.000288. URL: http://opg.optica.org/ol/abstract.cfm?URI=ol-11-5-288.

[17] Roland Koebler. *Optical trap unfocused*. [Online; accessed 14-July-2022]. 2011. URL: https://en.wikipedia.org/wiki/File:Optical_trap_unfocused.svg.

[18] Roland Koebler. *Optical trap focused*. [Online; accessed 14-July-2022]. 2011. URL: https://en.wikipedia.org/wiki/File:Optical_trap_focused.svg.

[19] A. Ashkin. “Forces of a single-beam gradient laser trap on a dielectric sphere in the ray optics regime”. In: *Biophysical Journal* 61.2 (1992), pp. 569–582. ISSN: 0006-3495. DOI: https://doi.org/10.1016/S0006-3495(92)81860-X. URL: https://www.sciencedirect.com/science/article/pii/S000634959281860X.

[20] Marco A. B. Andrade, Asier Marzo, and Julio C. Adamowski. “Acoustic levitation in mid-air: Recent advances, challenges, and future perspectives”. In: *Applied Physics Letters* 116.25 (2020), p. 250501. DOI: 10.1063/5.0012660. eprint: https://doi.org/10.1063/5.0012660. URL: https://doi.org/10.1063/5.0012660.

[21] Carl L Nave. *Magnetic Properties of Solids. HyperPhysics*. Tech. rep. Retrieved 2008-11-09, 2008.

[22] Zhi-An Ren et al. “Superconductivity and Phase Diagram in Iron-Based Arsenic-Oxides ReFeAsO1−x(Re = Rare-Earth Metal) Without Fluorine Doping”. In: *EPL (Europhysics Letters)* 83 (June 2008), p. 17002. DOI: 10.1209/0295-5075/83/17002.

[23] M V Berry and A K Geim. *Of flying frogs and levitrons*. 1997, pp. 307–313.

[24] Andre K. Geim. “Everyone’s Magnetism”. In: *Physics Today* 51 (1998), pp. 36–39.

[25] Igor Lyuksyutov, D. Naugle, and K. Rathnayaka. “On-chip manipulation of levitated femtodroplets”. In: *Applied Physics Letters* 85 (Oct. 2004), pp. 1817–1819. DOI: 10.1063/1.1781735.

[26] Hichem Chetouani et al. “Diamagnetic Levitation With Permanent Magnets for Contactless Guiding and Trapping of Microdroplets and Particles in Air and Liquids”. In: *Magnetics, IEEE Transactions on* 42 (Nov. 2006), pp. 3557–3559. DOI: 10.1109/TMAG.2006.880921.

[27] Hichem Chetouani et al. “Diamagnetic Levitation of Beads and Cells Above Permanent Magnets”. In: *Proceedings of the 14th International Conference on Solid-State Sensors, Actuators and Microsystems (Transducers Eurosensors ’07)* (June 2007). DOI: 10.1109/SENSOR.2007.4300230.

[28] David Garmire et al. “Diamagnetically Levitated MEMS Accelerometers”. In: July 2007, pp. 1203–1206. DOI: 10.1109/SENSOR.2007.4300352.

[29] Christian Pigot, Benoit Delinchant, and Gilbert Reyne. “Optimization of a 3D micro-accelerometer based on diamagnetic levitation”. In: *International Journal of Applied Electromagnetics and Mechanics* 30 (Sept. 2009). DOI: 10.3233/JAE-2009-1020.

[30] L. Liu and F. G. Yuan. “Nonlinear vibration energy harvester using diamagnetic levitation”. In: *Applied Physics Letters* 98.20 (2011), p. 203507. DOI: 10.1063/1.3583675. eprint: https://doi.org/10.1063/1.3583675. URL: https://doi.org/10.1063/1.3583675.

[31] Lei Liu and Fuh-Gwo Yuan. “Diamagnetic levitation for nonlinear vibration energy harvesting: Theoretical modeling and analysis”. In: *Journal of Sound and Vibration* 332 (Jan. 2013), pp. 455–464. DOI: 10.1016/j.jsv.2012.08.004.

[32] Sri Vikram Palagummi and Fuh-Gwo Yuan. “A bi-stable horizontal diamagnetic levitation based low frequency vibration energy harvester”. In: *Sensors and Actuators A Physical* 279 (July 2018). DOI: 10.1016/j.sna.2018.07.001.

[33] Stefan Clara et al. “An advanced viscosity and density sensor based on diamagnetically stabilized levitation”. In: *Sensors and Actuators A: Physical* 248 (July 2016). DOI: 10.1016/j.sna.2016.07.021.

[34] M. Boukallel, J. Abadie, and E. Piat. “Levitated micro-nano force sensor using diamagnetic materials”. In: *2003 IEEE International Conference on Robotics and Automation (Cat. No.03CH37422)*. Vol. 3. 2003, 3219–3224 vol.3. DOI: 10.1109/ROBOT.2003.1242086.

[35] S. Palagummi and F.G. Yuan. “An optimal design of a mono-stable vertical diamagnetic levitation based electromagnetic vibration energy harvester”. In: *Journal of Sound and Vibration* 342 (2015), pp. 330–345. ISSN: 0022-460X. DOI: https://doi.org/10.1016/j.jsv.2014.12.034. URL: https://www.sciencedirect.com/science/article/pii/S0022460X14010384.

[36] Chetvorno. *Eddy current brake diagram*. [Online; accessed 23-August-2022]. 2015. URL: https://en.wikipedia.org/wiki/File:Eddy_current_brake_diagram.svg.

[37] E. Simeu and D. Georges. “Modeling and control of an eddy current brake”. In: *Control Engineering Practice* 4.1 (1996), pp. 19–26. ISSN: 0967-0661. DOI: https://doi.org/10.1016/0967-0661(95)00202-4. URL: https://www.sciencedirect.com/science/article/pii/0967066195002024.

[38] P.J. Wang and S.J. Chiueh. “Analysis of eddy-current brakes for high speed railway”. In: *IEEE Transactions on Magnetics* 34.4 (1998), pp. 1237–1239. DOI: 10.1109/20.706507.

[39] Fausto Fiorillo. *Characterization and measurement of Magnetic Materials*. Elsevier Series in Electromagnetism. Elsevier Academic Press, 2004, p. 31.

[40] Chetvorno. *Eddy currents - explanation of drag force*. [Online; accessed 25-August-2022]. 2020. URL: https://en.wikipedia.org/wiki/File:Eddy_currents_-_explanation_of_drag_force.svg.

[41] Xianfeng Chen et al. “Diamagnetic composites for high-Q levitating resonators”. In: (Aug. 2022).

[42] I. Tiginyanu, V. Ursaki, and V. Popa. “10 - Nanoimprint lithography (NIL) and related techniques for electronics applications”. In: *Nanocoatings and Ultra-Thin Films*. Ed. by Abdel Salam Hamdy Makhlouf and Ion Tiginyanu. Woodhead Publishing Series in Metals and Surface Engineering. Woodhead Publishing, 2011, pp. 280–329. ISBN: 978-1-84569-812-6. DOI: https://doi.org/10.1533/9780857094902.2.280. URL: https://www.sciencedirect.com/science/article/pii/B9781845698126500105.

[43] M. Van Rossum. “Integrated Circuits”. In: *Encyclopedia of Condensed Matter Physics*. Ed. by Franco Bassani, Gerald L. Liedl, and Peter Wyder. Oxford: Elsevier, 2005, pp. 394–403. ISBN: 978-0-12-369401-0. DOI: https://doi.org/10.1016/B0-12-369401-9/00503-9. URL: https://www.sciencedirect.com/science/article/pii/B0123694019005039.

[44] Richard A. Lawson and Alex P.G. Robinson. “Chapter 1 - Overview of materials and processes for lithography”. In: *Materials and Processes for Next Generation Lithography*. Ed. by Alex Robinson and Richard Lawson. Vol. 11. Frontiers of Nanoscience. Elsevier, 2016, pp. 1–90. DOI: https://doi.org/10.1016/B978-0-08-100354-1.00001-6. URL: https://www.sciencedirect.com/science/article/pii/B9780081003541000016.

[45] Wei Han et al. “Toward Single-Atomic-Layer Lithography on Highly Oriented Pyrolytic Graphite Surfaces Using AFM-Based Electrochemical Etching”. In: *Nanomanufacturing and Metrology* 5.1 (Mar. 2022), pp. 32–38. ISSN: 2520-8128. DOI: 10.1007/s41871-022-00127-9. URL: https://doi.org/10.1007/s41871-022-00127-9.